TUNABLE FREQUENCY RESONATOR DESIGN AND REALIZATION

by

Yasemin Şen

B.S., Electrical and Electronics Engineering, Boğaziçi University, 2014

Submitted to the Institute for Graduate Studies in
Science and Engineering in partial fulfillment of
the requirements for the degree of
Master of Science

Graduate Program in Electrical and Electronics Engineering
Boğaziçi University
2018

ACKNOWLEDGEMENTS

First of all, I would like to express my deepest gratitudes to my advisor Professor Arda Deniz Yalçınkaya for his guidance through this path. Throughout the study, he gave me the learning opportunity to find a way to solve problems. Beside them, I would like to thank for his valuable lectures that constitute an origin for my special field of study. I would like to thank to Professor Onur Ferhanoğlu and Professor Sema Dumanlı Oktar for accepting taking a part in the evaluation committee.

Part of this thesis work was supported by Department of Scientific Research of Bogazici University (BAP) Project 16A02TUG4, I would like to thank for this support.

At the very beginning of this study, I could see the way of handling with experimental steps with the help of Emre, therefore I would like to thank to him and all people in MNCL laboratory for their guidence and help during experimental study. I would like to thank to our brother Ismail for his guidance and support. I also would like to express my deepest gratitudes to my friends Hacer, Vuslat, Fatma, and Duygu for their heartfelt support during this path.

From the beginning to this moment, I found my dear life friend Ali Alperen near me, feeling his love and understanding. I am more than grateful to him for his compassion and support.

I would like to express my deepest gratitudes to my parents Kazım and Habibe, my beloved sisters Gülhan and Mediha and my brother Halil İbrahim for their compassion and guidance. Throughout my whole life, I felt their support behind me, I can never repay them. I thank my family and my dear husband for everything I have.

ABSTRACT

TUNABLE FREQUENCY RESONATOR DESIGN AND REALIZATION

Oscillators are used to generate microwave signals in many electronic circuits in communication systems. Voltage controlled oscillators are also frequently found in electronic circuits. Resonance frequency is the determining factor of frequency band in oscillator constructions. Basically, when the resonance frequency of resonators can be adjusted by current or voltage control, then these resonators can be used in oscillator circuits instead of other structures mentioned in the literature. It has been foreseen in many studies that the resonance frequency and other factors affecting performance can be improved by the help of metamaterials' special properties and design variety. In this study, the design, manufacture and characterization of three resonator structures have been realized with the aim of obtaining tunable resonance frequency. In the first phase of the study; resonators are designed by examining the frequency effect of the results of capacitance variation obtained by conformal mapping and the other calculation methods of passive circuit elements. Three series of resonators were produced up to a certain stage using photolithography, nickel electroplating, metal sputter, selective wet etching and other auxiliary microfabrication processes. The fabricated resonators were characterized under magnetic excitation and without magnetic excitation. It was determined that the frequency was reduced by the applied magnetic force in the second series design. It is seen that the frequency in the steel resonator can be adjusted by 4.7 % with the applied voltage. The voltage and current were changed linearly and the resonator was characterized by measuring the displacement of the split cantilevers from their tips. 16 μm displacement of the tip of the cantilever results in 4.7% amount of frequency change.

ÖZET

AYARLANABİLİR FREKANSLI ÇINLAYICI TASARIMI VE GERÇEKLEMESİ

Osilatörler, haberleşme sistemlerinde yer alan birçok elektronik devrede mikrodalga işaretin üretilmesi amacıyla kullanılmaktadır. Frekansı uygulanan gerilim ile kontrol edilebilen osilatörler de elektronik devrelerde sıklıkla yer almaktadır. Çınlama frekansı osilatör yapılarında frekans bandını belirleyici unsurlardandır. Temelde, rezonans frekansı akım ya da gerilim kontrolü ile ayarlanabildiğinde, rezonatörler litaratürde belirtilen diğer yapıların yerine osilatör devrelerinde kullanılabilir. Rezonans frekansının ve performansı etkileyen diğer faktörlerin, metamalzemenin kendinden gelen özellik ve tasarım çeşitliliği ile geliştirilebileceği birçok çalışmada öngörülmüştür. Bu çalışmada rezonans frekansının ayarlanabilir olması hedeflenen üç rezonatör yapısının tasarımı, üretimi ve karakterizasyonu gerçekleştirilmiştir. Çalışmanın ilk aşamasında; rezonatörler, conformal mapping ve pasif devre elemanlarının hesaplama yöntemleri ile elde edilen kapasitans değişimi sonuçlarının frekansa olan etkisi incelenerek tasarlanmıştır. Fotolitografi, nikel elektrokaplama, metal kaplama, seçici ıslak aşındırma ve diğer yardımcı mikro-üretim işlemleri kullanılarak üç rezonatör serisi belirli aşamaya kadar üretildi. Üretilen çınlayıcılar, manyetik uyarımsız ve uyarımlı olarak karakterize edildi. Uyarı verilerek karakterizasyonu yapılan ikinci seri tasarımda manyetik kuvvet ile frekansın azaldığı belirlendi. Çelik çınlayıcıda frekansın uygulanan gerilim ile %4.7 oranında ayarlanabildiği görüldü. Gerilim ve akım doğrusal olarak değiştirilip, bölünmüş sundurmaların hareketi ölçülerek, çınlayıcının karakterizasyonu yapıldı. 16 μm hareket eden sundurma yapısının frekansta oluşturduğu değişim %4.7 oranındadır.

TABLE OF CONTENTS

LIST OF FIGURES

LIST OF TABLES

LIST OF SYMBOLS

A	Voltage gain
a	Side length of resonator
b	Respective value of the resonator end
c_i	Geometry dependent constants of inductance
C_{gap}	Gap capacitance
C_{surf}	Surface capacitance
cw	Width of cantilever
C_t	Effective capacitance
C_w	Curve in w plane
C_z	Curve in z plane
D_{avg}	Average diameter of inductance loop
D_i	Inner radius of inductance loop
D_o	Outer radius of inductance loop
D_w	Domain in w plane
D_z	Domain in z plane
E	Complex electric field
F_m	Mechanical force
f	Resonance frequency of the resonator
f_c	Carrier frequency
$f_{calculated}$	Calculated resonance frequency
f_{sim}	Simulated resonance frequency
f_{meas}	Measured resonance frequency
g	Gap width
$H(\omega)$	Transfer function
I	Direct current
K_{tune}	Voltage controlled oscillator gain
k_s	Spring constant
k	Geometry factor of gap capacitance

k'	Secondary geometry factor of gap capacitance
L_t	Effective inductance
l	Length of the electro coil magnetic stub
mg	Middle gap width
n	Number of turns of inductance loop
nw	Width of nested splits
Q	Surface charge
Q_r	Quality factor of resonator
r	Radius of curving cylinder of cantilevers in simulation
s_w	Width of the splits
s_l	Length of the splits
sw	Width of the split track
sl	Length of the split track
t	Thickness of resonator
V_0	Electric potential of resonator under electromagnetic field
V_{in}	Input voltage
V_{out}	Output voltage
V_{tune}	Tuning voltage
w	Frame width of resonator
δ	Amount of deflection in force applied spring
$\Delta\Phi$	Change in magnetic flux
Δt	Change in time
ϵ_{re}	Effective permittivity of resonator
ϵ_0	Permittivity of free space
λ	Line charge density
λ_r	Wavelength of resonator
μ_0	Permeability of the free air
μ	Permeability for electro coil
ρ	Fill ratio
σ	Surface charge density

Φ	Complex electric potential
ϕ	Real component of complex electric potential
ψ	Imaginary component of complex electric potential
ω_c	Angular carrier frequency
ω_0	Angular frequency of resonator

LIST OF ACRONYMS/ABBREVIATIONS

3D	Three Dimensional
AC	Alternating Current
BJT	Bipolar Junction Transistor
CMOS	Complementary Metal Oxide Semiconductor
CST	Computer Simulation Technology
DC	Direct Current
DI	De Ionized
FR	Flame Retardant
MEMS	Micro Electro Mechanical Systems
PCB	Printed Circuit Board
PR	Photo Resist
RF	Radio Frequency
UV	Ultra Violet
VCO	Voltage Controlled Oscillator
YIG	Yttrium Iron Garnet

1. INTRODUCTION

In any communication system including electronics circuits of test, measurement, radio, radar, television and warfare systems, a source of microwave signal is necessary. Sources of this microwave signal is generally termed as oscillators. To clearly define; an oscillator is a circuit that converts d-c power into a-c signal power using its natural capability of self-triggering [5, 6]. Although the definition that emphasizes the output of the oscillator circuit as an oscillating signal might bring to mind the amplifier circuit's similar output, in the operation of oscillators there is no need an input signal of excitation [7, 8]. There exists a number of parameters which have to be taken in to account in design and operation of an oscillator as a particular source of the electronic system.

Resonator blocks have a significant share in oscillator circuits and other microwave applications especially to decide the operating frequency [9, 10]. Signal is formed through the oscillator circuit and determining the frequency of oscillating signal is the duty of resonator part. Frequency range changes depending on RLC components of the resonator separately. If it is considered to make the frequency of the oscillator tunable, then the structure of the resonator must be changeable as a one option [11, 12]. In electronic circuits voltage controlled oscillators with controllable frequency resonators are used frequently, therefore design and realization of tunable frequency oscillator with controllable changing current / voltage is significant issue.

In this thesis, design and realization of tunable frequency resonator will be presented. Chapter II begins with general design considerations of resonator structures. Selection of resonator structure is specified in consideration of providing tuning of the frequency with changing design dimensions mechanically. Therefore, a theoretical background of square shaped split ring resonators are introduced and theoretical calculations of design parameters are explained with the conformal mapping method. Calculation of the capacitance and inductance values of resonator that will work between 2.5 GHz- 4.0 GHz frequency range is important to see the tuning range with mechanical change in frequency. From this point of view, resonance frequencies are calculated by hand. Studying resonance frequency by calculating capacitances procreate a new study that is explained in last two sections of Chapter II. Related simulations of dimensionally decided resonators are done with CST Microwave Studio Suite Design program as a primary study of the fabrication. In Chapter III, four different fabrication process of fabricated resonators are explained. Frequency measurements of fabricated devices for four different fabrication are discussed in Chapter IV and conclusion of this study is in Chapter V.

1.1. Oscillator Circuits

There are several approaches to design and realize oscillator circuits. One of the prevalent methods is to consider the oscillator as a positive feedback amplifier circuit. In this method, a low frequency oscillator circuit can be obtained, however at high frequencies just as in microwave oscillator circuits, the loop gain changes and the validity of the assumption of feedback network and amplifier do not load each other ends [13]. Negative resistance method is the second group of oscillator circuits in general aspect, that can provide a practical way to obtain reliable oscillations at higher frequencies. Although the second group has the name of negative resistance, if an electronic circuit generates sustained oscillation, it is seen that the circuit embraces a negative resistance regardless of whether it is a feedback oscillator circuit or negative resistance oscillator circuit. Its static or dynamic characteristics give birth to this property [14]. In these two groups of oscillators, one can generate a harmonic oscillation and therefore sinusoidal output signal. As distinct from, multivibrator and ring oscillators as relaxation oscillators, are sources of sawtooth and square wave oscillations.

The basic conceptual operation of an oscillator circuit can be explained from the linear feedback circuit. In the circuit, an amplifier with voltage gain A takes input V_{in} and produces the output V_{out}. At the same time, the output feeds back the input through the network with the frequency dependent transfer function $H(\omega)$ [15].

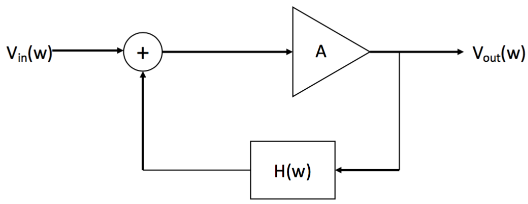

Figure 1.1. Block diagram of linear feedback path.

The output voltage can be expressed as

$$V_{out}(\omega) = AV_{in}(\omega) + H(\omega)AV_{out}(\omega). \tag{1.1}$$

If the equation is solved to yield the output voltage in terms of the input voltage,

$$V_{out}(\omega) = \frac{A}{1 - AH(\omega)} V_{in}(\omega) \tag{1.2}$$

It is seen that the denominator of the resulting equation must be zero at a specific frequency to achieve nonzero output voltage. Nonzero output voltage at a particular frequency means the circuit becomes an oscillator at that frequency. In summary;

$$|AH(\omega)| = 1 \tag{1.3}$$

$$\angle AH(\omega) = 2\pi n, n \in 0, 1, 2, ... \tag{1.4}$$

This is known as *Barkhausen Criterion* [16] . In an amplifier circuit, stability is the indispensable condition in contrast to the oscillation condition that requires the unstable nonzero output. At the beginning of operation, there must be a starting signal containing spectral component at the aimed frequency. This initial signal is obtained from the existing noise that comes naturally from the circuit itself. For instance, the effect of the temperature on components in the circuit, and causes noise signal which is called as thermal noise or white noise in general term [5]. The noise signal is amplified by the amplifier and it passes through the feedback component to be sent back to the input [17]. The frequency of continuing signal is determined by the resonator component in feedback network with the help of its bandpass characteristic. Initially, to provide the first oscillation from the noise signal, the output must show the growing behavior, hence the start up condition of gain and phase must be;

$$|A(\omega)H(\omega)| > 1 \tag{1.5}$$

$$\mathbf{arg}(A(\omega)H(\omega)) = 0 \tag{1.6}$$

Initially upon power up, this condition will be the case and signal will grow up until it reaches the limit level that is determined by the transistor operation. As the magnitudes of voltages and currents in the circuit increase, transistor of amplifier will attain the saturation, the gain will reduced and thus the circuit provides Barkhausen condition, therefore the circuit becomes an oscillator.

Feedback networks can be designed in two ways; one is to use resistors and capacitors and the other is to design with inductor, capacitor and resistors. Wien-Bridge oscillator and phase shift oscillator circuits are common in RC feedback network oscillator circuits and circuit model is very similar to the model in Figure 1.1. According to the design, feedback network is modified by resistor and capacitor components [18]. Second group of feedback oscillator circuits also named as resonant oscillators. In this class of oscillators, feedback is constructed with pure reactive π feedback network. Frequently used topologies can be listed as Colpitts, Hartley and Clapp oscillators.

Crystal oscillators are also widely used as RLC network of feedback helping to make the oscillator more stable and accurate. Mechanical and electrical structure of crystal oscillators creates the piezoelectric effect and with this crystal oscillators can have series and parallel resonance behavior. Briefly, when an AC voltage is applied across the crystal, the crystal vibrates at the frequency of applied voltage. Critical vibration occurs at the natural resonance frequency of crystal with the greatest value and this frequency depends on physical dimensions of crystal.

At microwave frequencies, negative resistance oscillators are useful. Negative resistance diodes or transistors are employed with passive load terminating device. Achievement of the sufficient negative resistance that compensates the losses of the passive circuitry is one of the most critical points of the negative resistance oscillator design. First of all, the transistor or diode in the circuit must be biased in active region. Then, sufficient impedance should be connected to produce feedback in the circuit. In steady state, the negative resistance produced by the active device -R should be equal to the loss resistance of the circuit. This negative resistance prevents exponential decay in the oscillating output signal. Furthermore, there must be the resonator part to determine the desired frequency of oscillation [19, 20].

1.2. Voltage Controlled Oscillator

The voltage controlled oscillator (VCO) used in electronic circuits of communication systems is a critical sub-block in case of tunable frequency by applied voltage is required. In VCO configurations depending on purpose of use and needs in the overall circuit. Bias control to change the gain of amplifier and capacitance as in the use of Colpitts oscillator, using voltage variable capacitors to tune resonator frequency and utilizing voltage variable resistors to change the gain of the circuit are generic approaches to create configurations [21, 22].

Varactor diodes can be used for second case. Depletion capacitance of the varactor diode is dependent on the reverse bias voltage across the diode. Altering the capacitance of the resonance circuit can be achieved by using varactor diode with a BJT oscillator circuit. In Figure 1.2 voltage dependency of capacitance of varactor diode is shown. A YIG (yttrium-iron-garnet) spheres can also be utilized for frequency tuning for a wide range by magnetic actuation. The problem is to build the equipment can be bulky and the response is rather slow [23].

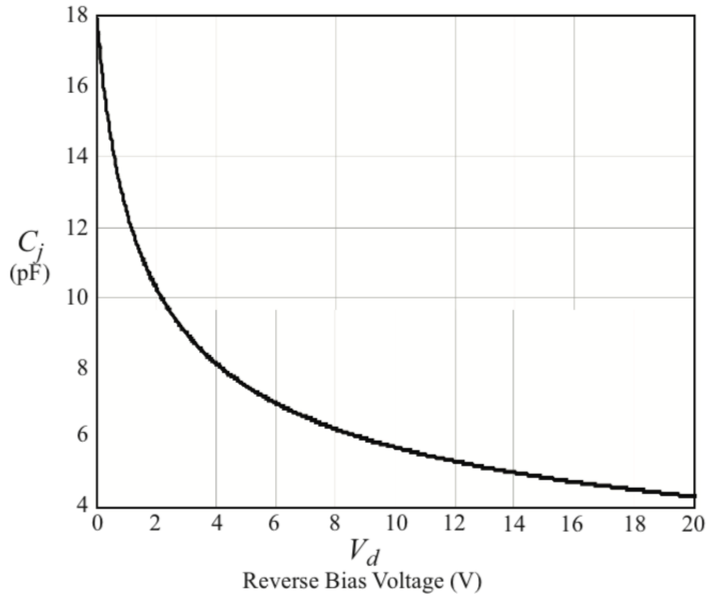

Figure 1.2. Capacitance as a function of reverse bias voltage for MV2102 varactor diode.

There exists some characteristics can be described as common among all. Stability, accuracy, low-noise and wide range of tuning with a well tuning gain come at the forefront of features in a VCO block [17, 24].

The resonator part forms the necessary resonance behavior in the circuits influences the performance of block in terms of specified features. Although the resonator component is the main theme of this thesis study, It would be satisfactory to briefly describe the fundamentals of the electronic behavior and two groups of VCO's before explaining the diversified configurations of resonators in VCO's and tuning mechanisms used.

A general VCO can be considered as a black box with an input V_{tune}, an output V_{out} and supply-ground terminals. V_{out} is an oscillating periodic output with angular carrier frequency ω_c. The angular frequency of the output is dependent on the tuning input voltage V_{tune} as a VCO requires [15, 25].

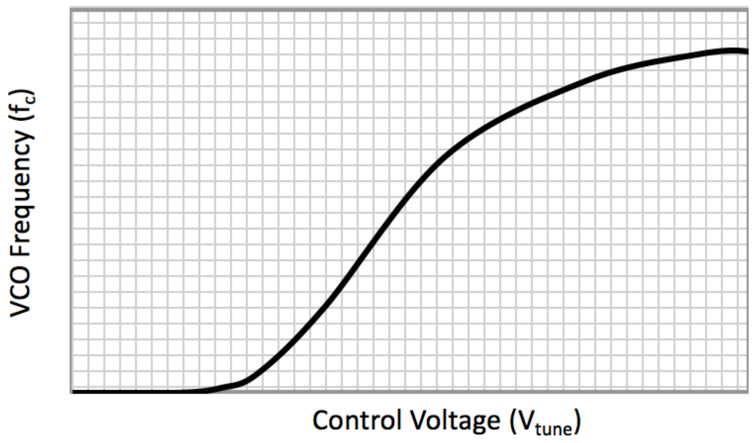

Figure 1.3. Oscillation frequency and tuning voltage.

$$V_{out}(t) = V_0 sin(\omega_c t + \phi) \tag{1.7}$$

$$\omega_c(V_{tune}) = 2\pi \times f_c(V_{tune}) \tag{1.8}$$

The gain of the circuit is obtained from the amount of frequency change with respect to the change in tuning voltage. Assuming linear change exist in a VCO block, the slope of the graph of linear relationship between f_c and V_{tune} gives the gain K_{tune}.

$$K_{tune} = \frac{df_c}{dV_{tune}} \tag{1.9}$$

1.3. Resonator Structures

Resonant circuits indicate band pass filter characteristic in frequency domain transfer function because of losses in the circuit. In the band pass characteristic, frequency selectivity of the circuit is measured with the quality factor. Quality factor is inversely related to bandwidth of the response, meanly higher quality factor is desired property to obtain narrow bandwidth and high frequency selectivity. The definition of the quality factor is actually represented with the ratio of energy stored in the resonator to the energy supplied. Capacitance, inductance and resistive losses form the function of quality factor. Quality factor equations for series and parallel resonant circuits are given in Equation 1.11 and Equation 1.12, respectively.

$$Q = 2\pi \frac{max\ energy\ stored}{energy\ lost\ per\ cycle} \tag{1.10}$$

$$Q = \frac{\omega_o \times L}{R} = \frac{1}{\omega_o CR} \tag{1.11}$$

$$Q = \frac{R}{\omega_o \times L} = \omega_o CR \tag{1.12}$$

Design, operation, employed materials, fabrication steps and frequency range of operation of resonator devices in oscillator circuits may change [5, 26]. LC tank resonators are composed of an inductive coil and a capacitor. The number of capacitor and inductor that will be used in the circuit depends on the selected topology. Integrated inductor and capacitors are also used as LC tank resonator as just in a transformer. Additionally, as it is explained in 1.1, quartz crystal is one option for resonator circuit that determines the oscillation frequency with active device.

Transmission lines can be used as resonators. Short and open circuited versions of half wave and quarter wave transmission lines represents parallel and series resonators. One port resonator device made from transmission line can be coupled to another resonator to obtain filter circuit or can be combined with the active network of oscillator circuit [27].

In high Q requirements, waveguide resonators can be counted as a good option. In its simplest form, waveguide resonators are metallic enclosures. Stored electric and magnetic energy provides required resonance behavior [28, 29]. Mode of excitation and box size are main considerations for better performance of resonator quality factor.

One of the most common used resonators is surface acoustic wave resonator and it is very similar to quarts crystals in use. One port surface acoustic wave resonator has one interdigital transducer and two reflectors. Interdigital transducer generates surface acoustic wave and reflectors reflects the wave and forms a standing wave between two reflectors and these three component of the device fabricated on quartz crystal [30]. Quartz crystal can also be used for the purpose of obtaining resonator device. Alternatively, the ceramic resonators are employed in many circuits as a cheaper option [31].

MEMS resonators are being increasingly employed in microwave circuits as an option for resonant frequency selectivity requirement. Capacitance of the resonator can be fabricated side by side with transistors that provides low noise performance. Using dielectric sandwich structure, cantilever beams or anchored and released capacitor architecture offers variable frequency with respectable quality factor [26, 32]. So many different capacitor structures can be fabricated with bulk and surface micro-machining techniques. Micro structures built from unusual materials provide new aspects of making resonators, and for micron size devices in CMOS technology [33, 34].

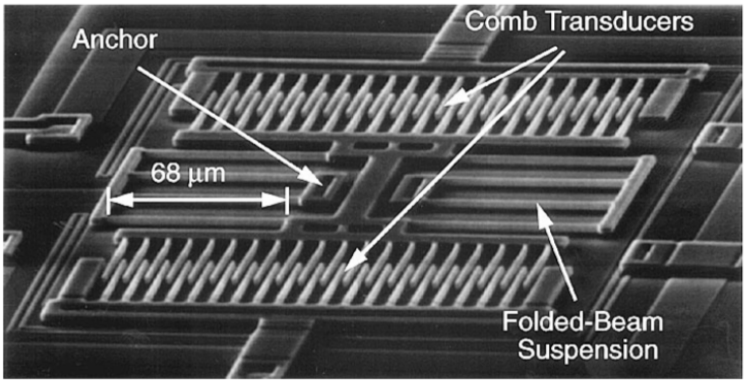

Figure 1.4. SEM of a 100-kHz folded-beam, capacitive-comb transduced resonator [1].

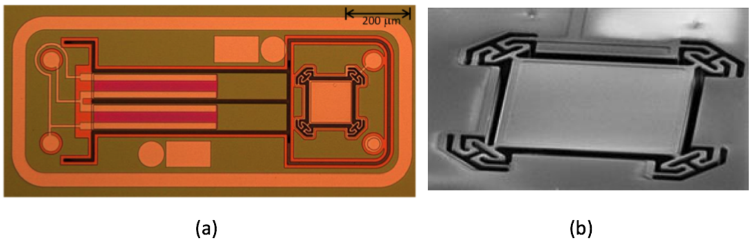

Figure 1.5. A micrograph of the fabricated chip. (a) oscillator. (b) resonator device on chip [2].

Inductors of MEMS resonators can also be fabricated on the same chip, however parasitic capacitance and lowered quality factor are main disadvantages. Electrical equivalent of the MEMS resonator can be considered as equal with spring - mass mechanical system, therefore realization of mechanical analysis can be asserted as a requirement. Applied mechanical force changes the geometry at that time, from this reason the electrical action changes [35]. There are so many examples on MEMS resonator structures for oscillators in progressing technology [36,37]. In Figure 1.4 and Figure 1.5, MEMS resonators fabricated by micro fabrication technologies is given as examples.

As it is mentioned in the first part of the thesis, the resonator in this study is designed as it has a movable structure to adjust the capacitance of the resonator and therefore to adjust the resonance frequency. There exist different devices explained in the first part used for the tuning of resonance frequency. These devices have advantages and disadvantages that are effective depending on the area of usage. The proposed resonator structure have main differences from the resonators of other studies [33, 34]. In the following words, different aspects and contributions of the proposed device is pointed.

- Extensive analysis of resonance frequency; in the first part an analysis on the frequency factors and tunable characteristic of resonators is studied. The method of capacitance calculation, specifically for the surface capacitance calculation is selected that the resulting frequency gives the closest information about the real frequency [38]. In many study, separate calculation for the surface capacitance is not considered because of complexity. However, the method that is explained with conformal mapping technique is applicable for different resonator designs.
- Composition of magnetic actuation and mechanical response; mechanical tuning of the design is used in MEMS devices, and actuation mechanism is electrothermal, electromechanical and piezoelectrical as in [2]. In this work, magnetic force is applied and the mechanical change result in the change of shape. The proposed resonator device is a combination for magnetic force, mechanical deflection and frequency shift.
- Millimeter scale resonator designs; resonator dimensions are designed in millimeter and centimeter range. These dimensions are important for fabrication and characterization procedures. In MEMS devices and improved varactor diodes, fabrication require highly developed clean room and process machines. Also, characterization or even simple frequency measurement have to be done with a special setup. The proposed device, can be fabricated with fabrication machines in the clean room of the school and also the last design can be fabricated with a laser cutting machine. Also materials are not expensive and rare. Measurement is also not complicated for resonators, because in current facilities frequency, deflection and applied actuation could be obtained.
- Material variety; nickel electroplated copper, nickel on gold with tango black and

stainless steel materials are used. In many applications, these metals aren't used for resonators. Semiconductors are used frequently, however nickel and ferritic steel are both considerable choices for resonators in high frequency range. In this work, a material variety and experimental outcomes are also explained.

- Frequency tuning band; the tuning band of the resonance frequency depends on the mechanical dimensions of the resonator [12]. Actually, in the proposed structure and in the last device, frequency can be tuned with greater amount with the same current application. This is depends only on the shape and width of the cantilevers. So that, to have a larger amount of change it is enough to make different shape or narrow cantilever. In some of other devices, the tuning range is constant and the only method is to change the material or all design.
- Good quality factor; the measured device has a good quality factor explained in results part. In tunable devices, the quality factor decreases with changing frequency in general. Also for higher frequency applications obtaining high quality factor is not easy. So that, the resulting device has a good and stable quality factor that is proper to use in oscillator and filter applications [39].
- In mentioned studies, resonator is designed according to the specified frequency range [22]. The tuning the resonance frequency is applied with varactor diode. To be able to tune the device varactor diode is necessary. In this work, tuning and resonance behavior is combined with a simple one layer steel device. The material is durable and resistant to many external effects.
- Lastly, this device can be integrated to a chip of for example filter by using the metal layers on the chip. Metals are formed at the end of all process steps so that the device can be fabricated on the chip without any damage. Inevitably, dimensions, shapes and application of the magnetic force might be changed.

2. DESIGN

Various designs of resonators have variety of usage in electronic systems as a part of filters, oscillators, voltage controlled oscillators, sensor and actuator systems. MEMS fabrication methods can be employed to materials with micron size dimensions, therefore restrictions on designs can be eliminated by this way. Movable strips of MEMS structures allow to make tunable capacitance and inductance values in resonators. Because of their unique electrical and magnetic properties, metamaterials become popular in MEMS resonators.

Metamaterials are artificial composites comprising a periodic array of subwavelength constituents with their extraordinary electromagnetic properties such as negative permittivity, negative permeability and negative refractive index [40, 41]. A single element of metallic metamaterial array can be considered as an LC resonant circuit. Unit cell size and dimensions of designed structure is critical to ensure desired capacitance and inductance values [42, 43]. Metamaterial resonators promise opportunities [44] for investigation of diversified applications interpolating superlenses, invisibility cloaks, absorbers and sensors [45, 46].

Split ring resonator can be like cylindrical, square, hexagonal or other geometric shapes together. The importance of its shape is related to its effectuated capacitance and inductance. Metamaterial split ring resonators can be counted as unified field of mentioned studies. In [47–51] some critical points related to the subject of this thesis have been studied.

In this study, our aim is to design split ring resonators and making resonators tunable by released movable splits utilizing micro structure fabrication methods. Two of square shaped split ring resonator is selected in this thesis and configurations of designed resonators are given in Figure 2.3. In Figure 2.1, geometrical parameters of

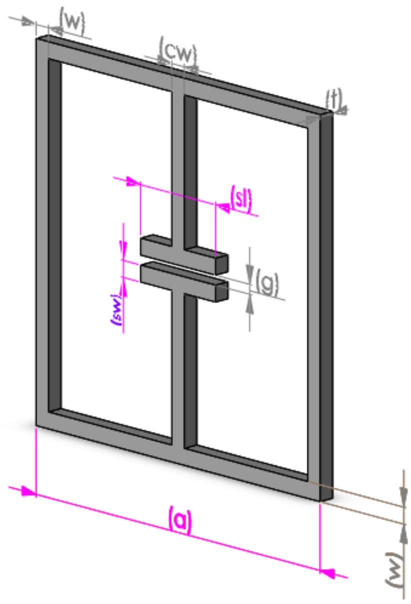

Figure 2.1. Single gap resonator structure and geometrical parameters.

sample structure are displayed.

Geometrical parameters of designed resonators change depending on design structure, therefore there will be more parameters listed in detail for each of designed resonators in addition to the main skeletal structure. a stands for the side length of the square resonator unit cell. w stands for the width of the resonator frame and cw stands for the width of the cantilever that comes out from the middle of the frame. sw stands for the two split tracks and g stands for the gap between these two split tracks. Number of gaps and split tracks are different in nested gap resonator design; however the geometry of the resonator is designed in a **x** direction symmetry, therefore one additional parameter nw which represents the width of nested splits is enough to explain the geometry. Lastly, t stands for the thickness of the resonator. In Figure 2.2, mg stands for the gap in the middle of nested splits and nw stands for nested split widths. Widths of nested splits are equal through the L shaped extensions.

Dimensions of these two resonators are decided to provide the range of resonance frequency between 1 GHz and 4 GHz. The proposed geometry of resonator in [44] is

Table 2.1. The characteristics of first generation resonator structure.

	Side Length (a)	Width of the Frame (w)	Thickness (t)	Cantilever Width (cw)	Width of the Split Track (sw)	Length of the Split Track (sl)	Gap (g)
Single Gap Split Ring Resonator	11.4 mm	0.5 mm	0.35 mm	0.5 mm	0.5 mm	4.55 mm	0.3 mm

selected as a guide for the first step of the design study. Geometrical dimensions are redesigned to meet the desired resonance frequency. To increase the frequency, feature size is increased and the size of the gap is decided according to specified calculation method in this thesis and simulations. After dimensions of single gap resonator are decided, nested gap resonator is designed intercalarily .

Table 2.2. The characteristics of first generation nested gap resonator structure.

	Side Length (a)	Width of the Frame (w)	Thickness (t)	Cantilever Width (cw)	Width of the Split Track (sw)	Length of the Split Track (sl)	Gap (g)	Middle Gap (mg)	Width of Nested Splits (nw)
Nested Gap Split Ring Resonator	11.4 mm	0.5 mm	0.35 mm	0.5 mm	0.5 mm	2.0 mm	0.3 mm	0.3 mm	0.3 mm

Bended states of resonators are shown in Figure 2.4. To construct the structure in consideration of bending response is significant for our capacitance tuning purpose. The two cantilevers in the middle of the resonators behave like a spring with spring constant value k_s.

In theory, spring constant, applied force and amount of displacement is related with the Equation 2.1. In our case, force is magnetic force applied from the magnetic coil in the measurement setup. To calculate the spring constant, moment of inertia, stress and strain values for the material at this condition can be used. The detailed explanation about this calculation procedure is in [52, 53]. The cross-section of cantilever

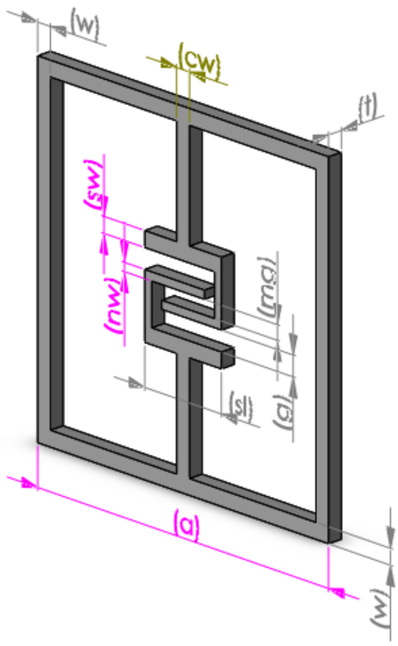

Figure 2.2. Nested gap resonator geometrical parameters.

spring feature is in Figure 2.5

$$F_m = \mathbf{k_s} \times \delta \tag{2.1}$$

Because of the problem in release step of cantilevers in fabrication of resonators, small perforations are added to the second design, in Figure 2.6. It is assumed that these little holes do not affect the tuning of the capacitance. Perforations exist only in cantilevers from the beginning of part to be released. There is a small portion left as unperforated toward to the end of the cantilever for the photoresist because of the possibility of undercutting during the etch step. Detailed information about the fabrication process will be given in Chapter 3.

3D-generated resonator is the third type of studied structures. In this generation, only the single gap split ring resonator is designed because the feature size of the nested

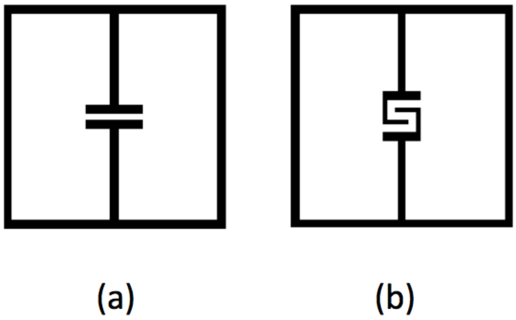

Figure 2.3. The two designed resonator structures. (a) single gap split ring resonator. (b) nested gap split ring resonator.

gap resonator structure is too small to fabricate with this method. As it can be seen from the Figure 2.7, organization is raised with a thin plate square piece. The purpose of raising is to make cantilevers released and far from the bottom retainer. Square piece is added for connecting necessary cables during fabrication to be torn off after related fabrication step is finished.

Lastly, four different designs are evolved. Steel material and measurement setup are taken into account and therefore the area of the conformation. In Figure 2.8, (a) and (b) are similar to first generation resonators. Thin and thick anchors are joined that third (c) and fourth (d) designs are formed. Lastly, because of we have enough area for this generation, conjugate or complementary version of a discrete two gap resonator is designed and simulated, (e). Complementary version of the two gap split ring resonator has different dimensions than the other designs, therefore it is better to present structural parameters of the complementary resonator, in Figure 2.9.

2.1. Theoretical Background

As a first step in design of the SRR device, it must be taken into account that the metamaterial underlying the resonator device operate properly in the effective-medium regime [54]. It means that the unit cell size should be much smaller than the quarter wavelength $\frac{\lambda_r}{4}$. λ_r is resonant wavelength of the resonator. As the lattice

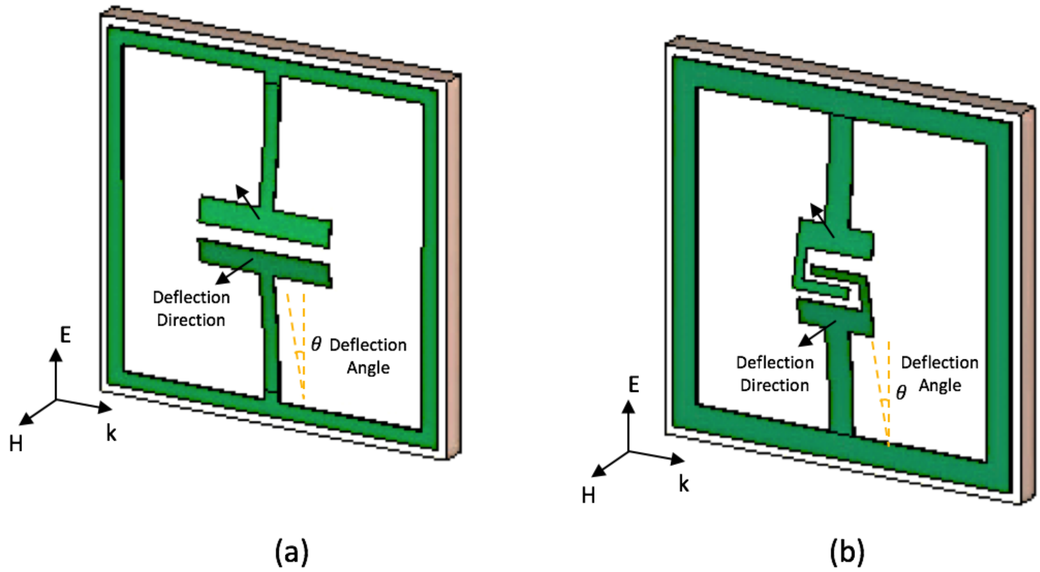

Figure 2.4. Bending simulation of designed resonator structures. (a) single gap split ring resonator with bending splits. (b) nested gap split ring resonator with bending splits.

constant and quarter wavelength become closer than the effect of diffraction increases with decreasing refraction.

Single gap split ring resonator and its electrical equivalent is illustrated in Figure 2.10. The resonator ensures pure electric resonance, because the collective magnetic flux is nullified by the impact of resonator symmetry. Due to the relation between wavelength and the unit cell size, the resonator can be considered as an LC resonance circuit. The gap between split tracks in the resonator forms the capacitance and two loops of two symmetric sides results in inductance components [55, 56]. Electric field polarization is perpendicular to the gap, therefore the capacitance is excited to generate electric resonance in the operation of the resonator.

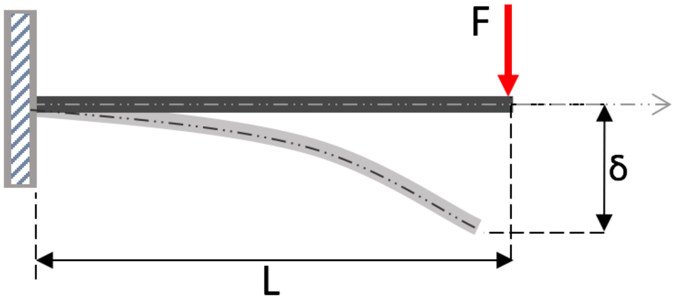

Figure 2.5. Spring - applied magnetic force to the resonator cantilevers.

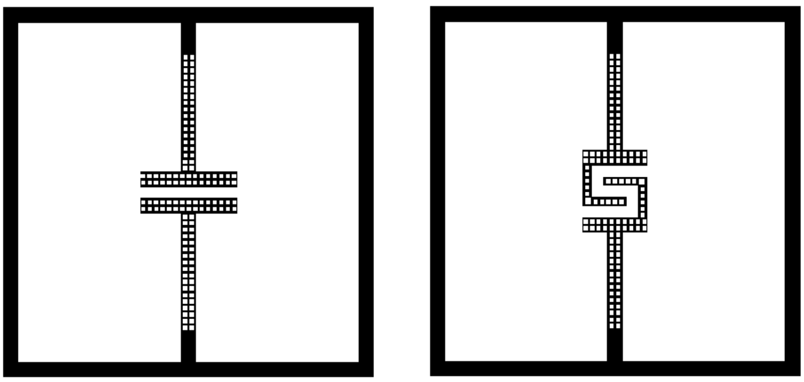

Figure 2.6. Perforated resonator structures. (a) single gap perforated split ring resonator. (b) nested gap perforated split ring resonator.

Resonance frequency is calculated using the formula in Equation 2.2. $\mathrm{L_t}$ and $\mathrm{C_t}$ represents equivalent inductance and capacitance values respectively [17].

$$\mathrm{f} = \frac{1}{2\pi \times \sqrt{\mathrm{L}_t \mathrm{C}_t}} \tag{2.2}$$

Inductance of the resonator can be calculated using Equation 2.3, that is provided in [4] as the general formula for an arbitrary shaped inductor. As the shape changes coefficients provided differ. In our case, coefficients in the equation benefit from is

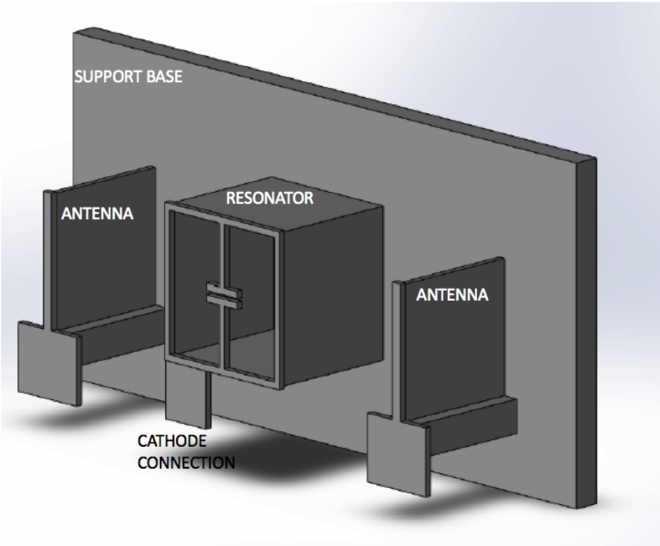

Figure 2.7. 3D-generated resonator.

taken as in the case of square shaped inductor.

$$\mathrm{L_t} = \frac{\mu_0 n^2 D_{av} c_1}{2}[\ln\frac{c_2}{\rho} + c_3\rho + c_4\rho^2] \tag{2.3}$$

In the Equation 2.3, μ_0 is the permeability of the free space that is $4\pi \times 10^{-7}$ Tm/A. n stands for number of turns, D_{av} stands for average diameter that can be calculated as in Equation 2.4 and ρ is the fill ratio. Equation 2.5 provides ρ calculation. D_o and D_i represents outside and inside diameter of the inductor. Lastly, c_i stands for coefficients that are presented in Table 2.3.

$$\mathrm{D_{av}} = \frac{D_o + D_i}{2} \tag{2.4}$$

$$\rho = \frac{D_o - D_i}{D_o + D_i} \tag{2.5}$$

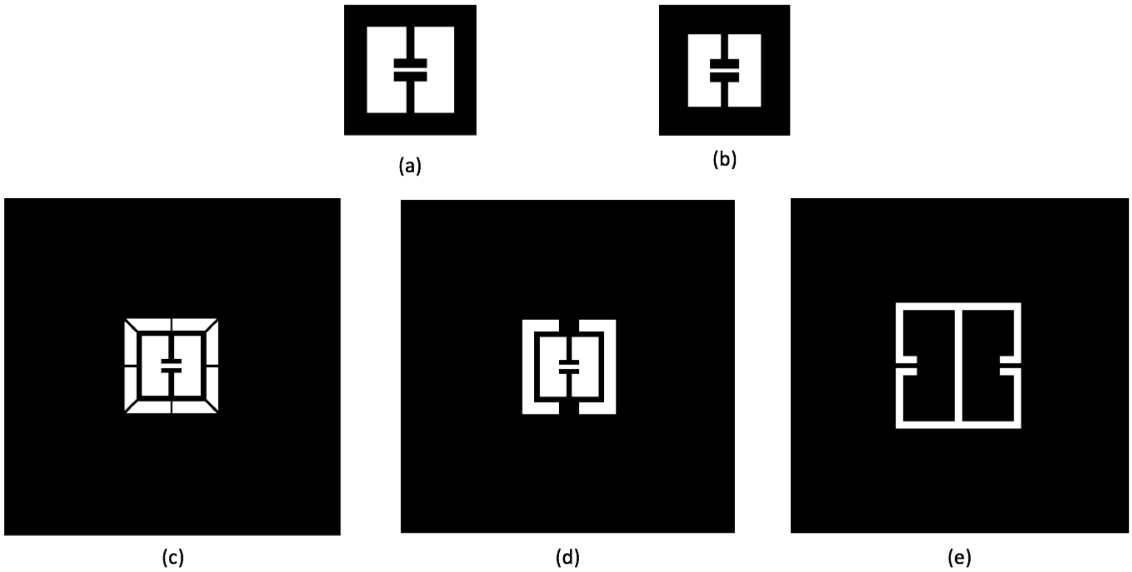

Figure 2.8. Anchored and nonanchored series of resonator structures proper to fabricate with steel material. (a) single gap resonator-1. (b) single gap resonator-2. (c) thin anchored single gap resonator. (d) thick anchored single gap resonator. (e) complementary version of two gap resonator.

The capacitance coming from the gap is not the only capacitance in the resonator device, because the charges in the gap are not the individual source of capacitance. Surface charges beget an additional capacitance named as surface capacitance [38]. For the inductance of the resonator, effective inductance is considered. Since gap capacitance C_{gap} and surface capacitance C_{surf} are in parallel equivalent capacitance C_{t} is given as in Equation 2.6.

$$C_t = C_{\mathrm{gap}} + C_{surf} \tag{2.6}$$

When we look at two capacitance separately, the capacitance caused by the gap that is narrow enough to make parallel plate capacitor assumption. Using Equation 2.7, gap capacitance can be calculated with the fringing capacitance effect in a detailed form [42].

	Side Length (a)	Length of the Frame (a_i)	Thickness (t)	Cantilever gap (g)	Cantilever Length (l_o)	Inner Flank (s_i)	Outer Flank (s_o)
Complementary Split Ring Resonator	55 mm	20 mm	0.6 mm	0.5 mm	3.25 mm	7.5 mm	9.5 mm

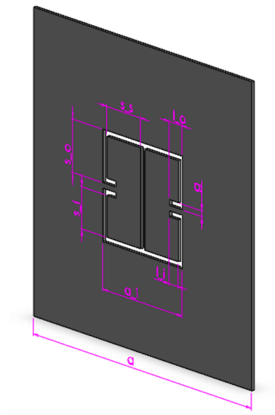

Figure 2.9. Two gap complementary resonator structure and dimensions.

Table 2.3. Coefficients for general inductance expression [4].

Geometry	c_1	c_2	c_3	c_4
Square	1.27	2.07	0.18	0.13
Hexagonal	1.09	2.23	0.00	0.17
Octagonal	1.07	2.29	0.00	0.19
Circle	1.00	2.46	0.00	0.20

$$\mathrm{C}_{gap} = \frac{\varepsilon_{re} \cdot 10^{-3}}{18\pi} \cdot \frac{\mathrm{K(k)}}{\mathrm{K'(k)}} \mathrm{s_l} \tag{2.7}$$

where ε_{re} is the equivalent permittivity, $\mathrm{s_l}$ is the horizontal length of the gap. $\frac{\mathrm{K(k)}}{\mathrm{K'(k)}}$ is extracted from following three equations.

$$\mathrm{k} = \tan^2 \cdot \frac{[0.25 s_w \pi]}{(s_w + g)} \tag{2.8}$$

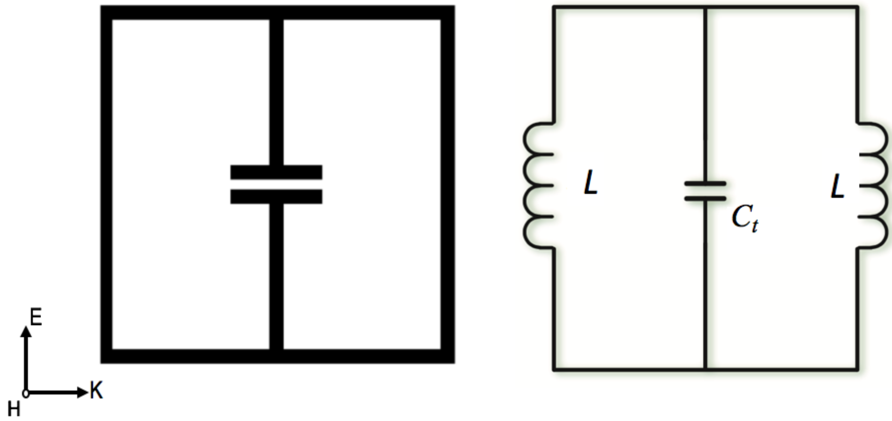

Figure 2.10. Electrical equivalent of sample model resonator.

$$\mathrm{k}' = \sqrt{1 - \mathrm{k}^2} \tag{2.9}$$

$$\frac{\mathrm{K(k)}}{\mathrm{K(k')}} = \frac{\pi}{\ln\left(2\frac{1+\sqrt{\mathrm{k}}}{1-\sqrt{\mathrm{k}}}\right)} \tag{2.10}$$

Equivalent relative permeability used in Equation 2.7, can be calculated from Equation 2.11 [42].

$$\varepsilon_{re} = \frac{\varepsilon_r + 1}{2} + \frac{\varepsilon_r - 1}{2} \cdot \frac{1}{\sqrt{1 + 12\frac{t}{w}}} \tag{2.11}$$

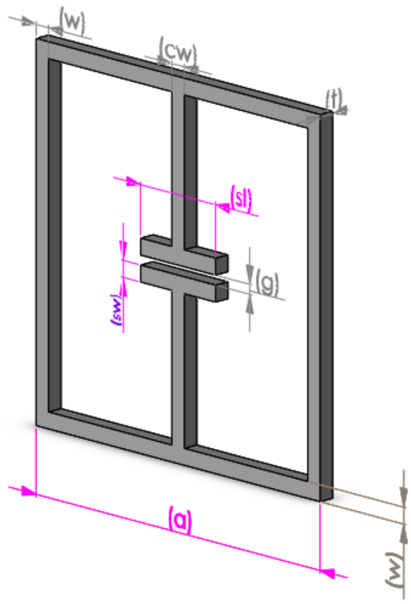

Figure 2.11. Single gap resonator structure and geometrical parameters.

In Equation 2.8, s_w and g represents the width of the splits and the gap respectively as it is shown in Figure 2.11. The thickness of the resonator layer is entitled as t.

Equations explained for the gap capacitance calculation can also be used for the nested gap structure multiplying the resulting capacitance calculated with this method as a single gap resonator with 3, which represents the effect of having intertwined.

The thorny part of these computations that should be solved is surface capacitance. Because the structure is subject to both effects of surface and gap, the surface capacitance is significant as the gap capacitance. To be able to express the necessary surface capacitance formula in this structure that is different by genre, a method named as *Conformal Mapping* is concentrated on. In the Subheading 2.1.1, conformal mapping method and in Subheading 2.1.2 surface capacitance calculation will be explained.

2.1.1. Conformal Mapping

Conformal mapping is a mathematical technique used to map a mathematical problem of complex variables into another. Conformal mappings can be utilized to solve Laplace equation on complicated planar domains that comes out in various physical problems, as in [57, 58]. Complex analysis forms a basis for conformal mapping study [3].

Transformations of mathematical problems via conformal mapping encompass the knowledge of all about complex numbers, however the corner stone of the complex function theory is the complex derivative and its relation to the harmonic functions [23]. To be able to obtain required information from the complex derivative, we must notice the *Cauchy − Riemann* equations with the derivation theorem [59].

Theorem 2.1. *A complex function f(z) = u(x,y)+*$\mathbf{i}$*v(x,y) depending on z = x +* $\mathbf{i}$*y has a complex derivative f'(z) if and only if its real and imaginary parts are continuously differentiable and satisfy the Cauchy-Riemann equations.*

$$\frac{\partial u}{\partial x} = \frac{\partial v}{\partial y}, \qquad \frac{\partial u}{\partial y} = -\frac{\partial v}{\partial x}.$$

If we look at harmonic functions, the relation between complex derivative and them can be summarized as follows;

Theorem 2.2. *If f(z) = u(x,y)+*$\mathbf{i}$*v(x,y) is any complex analytic function, then its real and imaginary parts, u(x,y), v(x,y) are both harmonic functions.*

In the combination of complex potentials, harmonic functions and conformal mapping by considering required boundary value conditions, when the values of the harmonic function (for example temperature, voltage) are given in the specified geometry, then the values of the harmonic function on the surface of the geometry can be found. This is the idea behind our computation of surface capacitance of the resonator [60].

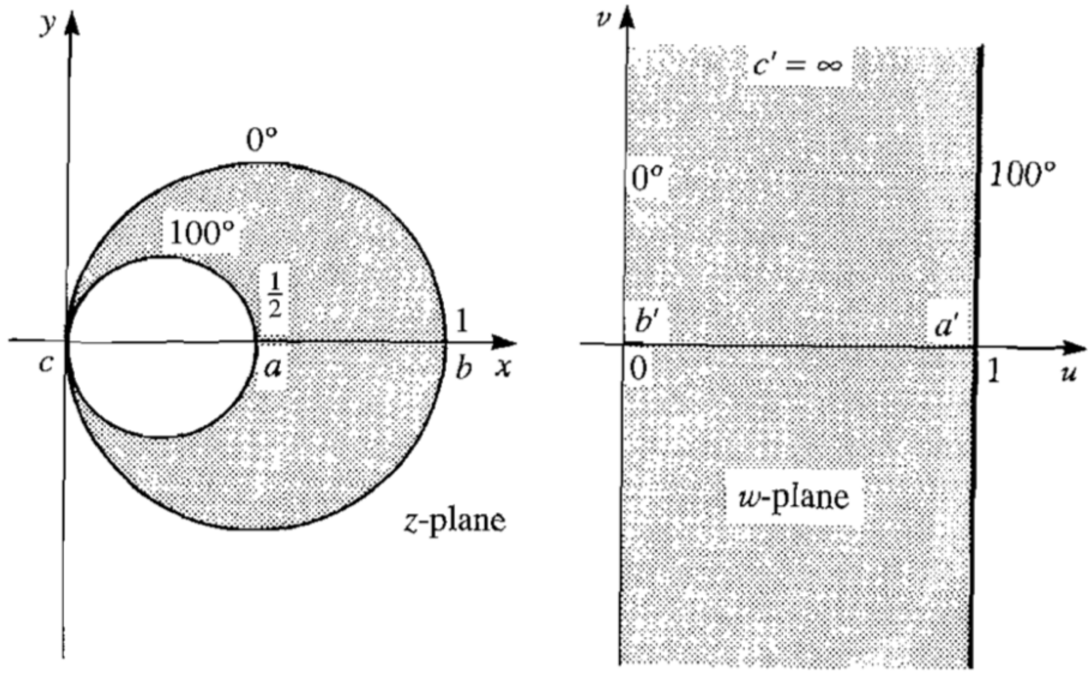

Figure 2.12. Harmonic function example [3].

As an example, the calculation of the temperature between two cylinders separated by an infinitesimal gap at the origin in z - plane can be considered. The harmonic function of temperature is $\phi(x, y)$ and two dimensional view is in Figure 2.12. After the transformation is applied to the complicated structure of two cylinders, the shape of the domain becomes clear and boundaries are simpler.

Once $\phi(u, v)$ is obtained from the mapped domain and the transformation equation, attaining the $\phi(x, y)$ and $\psi(x, y)$ which are the real and imaginary parts of the overall complex temperature function is trivial. Just applying the inverse transform on $\phi(u, v)$ provides the z - plane equivalent of the temperature function.

A function of complex variable z cannot be studied by conventional graphing procedure of algebra. Two planes, z - plane with axes x, y and w - plane with axes u, v are used instead of this. If the relation between z and w is represented by $w = f(z)$, then it means that $f(z)$ sets up the correspondence between points in the z - plane

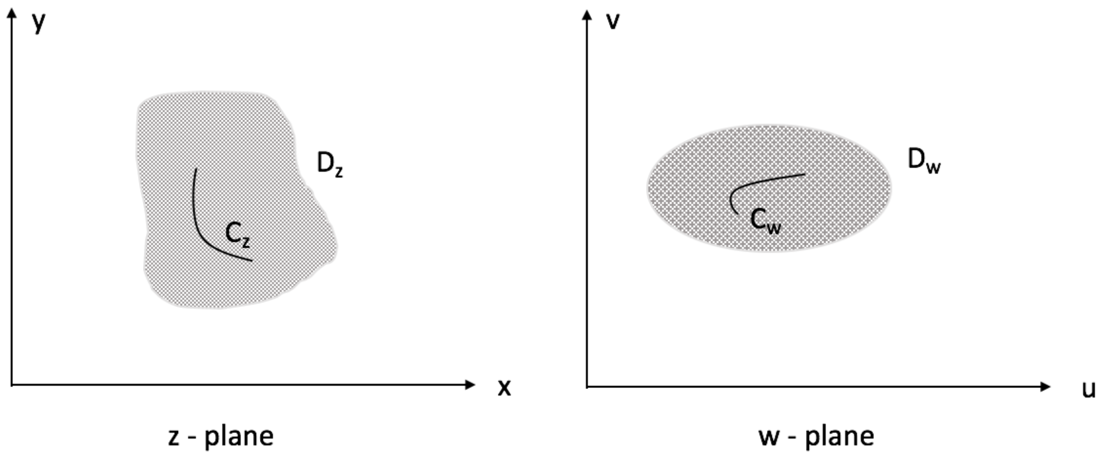

Figure 2.13. $w = f(z)$ transformation on domain and curve.

and w - plane. Meanly, to each value of z in the region there will correspond a value of dependent variable w; therefore, w is a function of z [61].

When all the points lying in a domain D_z of the z - plane is mapped by the function $w = f(z)$, there will be formed a domain D_w in the w - plane. Transformation of the D_z domain to the D_w is characterized as mapping. Similarly, if a curve C_z in the domain D_z is mapped to the w plane with its all points, then a curve C_w will be constructed. In Figure 2.13, explained mapping on planes is illustrated.

It is quite difficult to explain a comprehensive topic with this much information, nevertheless it is enough to get general requisite information for our theoretical approach.

2.1.2. Surface Capacitance Expression

To be able to express the surface capacitance in a plane the information of the total charge of the surface, therefore the surface charge density is necessary. Surface charge density is proportional to the imaginary component of the electric field due to the fact that the imaginary part of the complex potential represents the stream

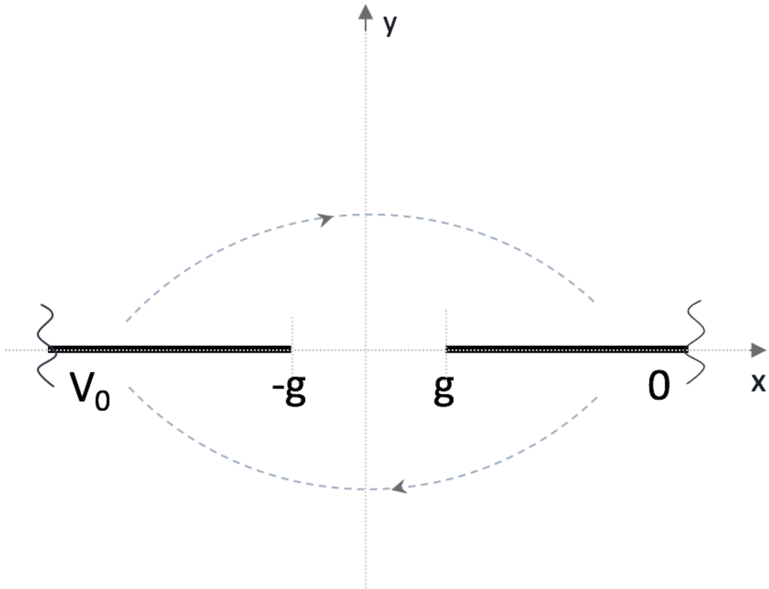

Figure 2.14. Two semi-infinite plane with gap *2a*.

function which is responsible from perpendicular stream lines to the equipotentials in the aforementioned plane. In our structure, there exist two case must be considered in calculations. The first one is two planes with a measurable gap and the second is planes separated by an infinitesimal gap.

In Figure 2.14, two semi-infinite planes are illustrated. The gap divides them in *2a* width and one of the planes is at V_0 potential and the other is at zero potential. The curved line above and below represents the electric field between the two planes.

Complex potential which is $\Phi(z)$ for two semi-infinite planes that are separated by a gap of $2a$ is given in the Equation 2.12. z is the complex variable of the complex potential function. The relation between complex electric field and the complex potential results in the electric field expression, in Equation 2.14.

$$\Phi(z) = \frac{V_0}{\pi} \cos^{-1}\left(\frac{z}{g}\right) \tag{2.12}$$

$$E(z) = \frac{-d\overline{\Phi(z)}}{dz} = \frac{-d}{dz}\overline{\left(\frac{V_0}{\pi}\cos^{-1}\left(\frac{z}{g}\right)\right)} \tag{2.13}$$

$$E(z) = \frac{V_0}{\pi g}\overline{\left(\frac{1}{\sqrt{1-\left(\frac{z}{g}\right)^2}}\right)} \tag{2.14}$$

From the electric field expression and the relation to the surface charge density, in Equation 2.15, we find the corresponding surface charge density as 2.18. At the intermediate steps of the calculation, complex electric field rewritten in a detailed form to obtain the imaginary part. The importance of the imaginary part is to be able to use stream function which gives required physical description about the surface charge.

$$\sigma = 2\varepsilon_0\left[Im(E(z))\right] \tag{2.15}$$

$$E(z) = \frac{V_0}{\pi g}\left[\left(\overline{\frac{-1}{\sqrt{1-\left(\frac{x+iy}{g}\right)^2}}}\right) + 2Re\left(\overline{\frac{1}{\sqrt{1-\left(\frac{x+iy}{g}\right)^2}}}\right)\right] \tag{2.16}$$

$$Im(E(z)) = \frac{V_0}{\pi g}\left(\frac{1}{\sqrt{\left(\frac{y}{g}\right)^2-1}}\right) \tag{2.17}$$

Using all of expressions above, the surface charge density σ;

$$\sigma = \frac{2\varepsilon_0 V_0}{\pi g}\left(\frac{1}{\sqrt{\left(\frac{y}{g}\right)^2-1}}\right) \tag{2.18}$$

Primary purpose of these calculations is to acquire the total charge information, therefore the computation continues with the linear charge density expression;

$$\lambda = \int_g^b \sigma dy \tag{2.19}$$

Linear charge density is the integral of surface charge density along the surface boundary of two sides. At this point, boundaries are selected as a and b such that a is the beginning of the plane and b stands for the ending dimension of our structure.

$$\lambda = \frac{2\varepsilon_0 V_0}{\pi}\left[\log\left(\frac{b}{g} + \sqrt{\left(\frac{b}{g}\right)^2 - 1}\right)\right] \tag{2.20}$$

Total charge from the linear charge density is trivial, and in Equation 2.21 t stands for the thickness and w stands for the width of the structure.

$$\mathrm{Q} = (t + w)\lambda \tag{2.21}$$

If we calculate the capacitance from the total charge with known potential using the principal capacitance relation, in Equation 2.22; resulting expression provides the surface capacitance equation of the two plane separated with the gap $2g$.

$$\mathrm{C} = \frac{\mathrm{Q}}{\mathrm{V}_0} \tag{2.22}$$

$$\mathrm{C} = \frac{2\varepsilon_0}{\pi}\left[\log\left(\frac{b}{g} + \sqrt{\left(\frac{b}{g}\right)^2 - 1}\right)\right](t + w) \tag{2.23}$$

In Figure 2.15, two semi-infinite planes with infinitesimal gap in the middle. The infinitesimal gap is actually not exist when the resonator is not working. Under operation with the wave, because of the charge localization, there exist an infinitesimal gap that is not charged, forms a vacancy line. Considering this effect on the side frame

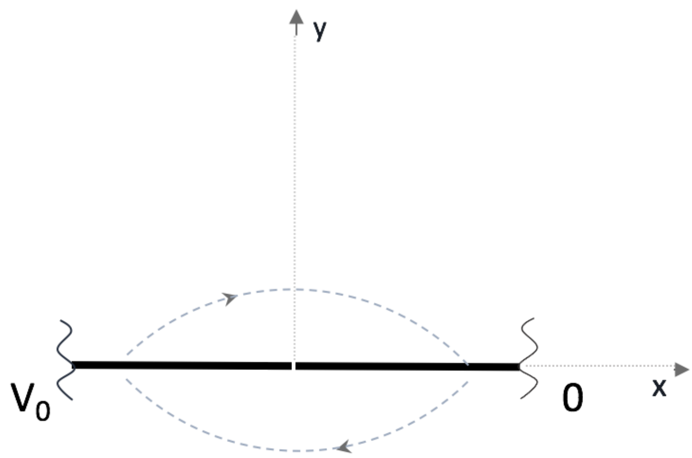

Figure 2.15. Two semi-infinite plane with infinitesimal gap.

of the resonator, additional surface capacitance component coming from sides can be calculated [3]. The curved line above and below represents the electric field between the two planes, and one side is at V_0 and the other is at $-V_0$.

The device is fabricated on glass-reinforced epoxy laminate sheet, FR-4; therefore, for the surface potential of the frame of the resonator, we can analyze and calculate the complex surface potential just for the upper half plane. For the upper half plane, Poisson Integral Formula is applicable as for the harmonic functions. In the Equation 2.24, Poisson Integral Formula for the upper half plane including both real and imaginary parts is shown. Because we need the surface charge density, electric field from the electrostatic potential $\phi(x, y)$ is construed as in the case of separated planes.

$$\phi(x, y) + i\psi(x, y) = \frac{y}{\pi} \int_{-\infty}^{\infty} \frac{\phi(u, 0) + i\psi(u, 0)}{(u-x)^2 + y^2} du \tag{2.24}$$

In Equation 2.25, real parts of both sides are equated. Solving the integral with the necessary boundary values, electrostatic potential for the upper half plane confronts as in Equation 2.26.

$$\phi(x,y) = \frac{y}{\pi}\int_{-\infty}^{\infty} \frac{\phi(u,0)}{(u-x)^2+y^2}\,du \tag{2.25}$$

$$\phi(x,y) = V_0 - \frac{2V_0}{\pi}\tan^{-1}\frac{y}{x} \tag{2.26}$$

Electric field is the inverse derivative of the electrostatic potential as we used in first calculation, and surface charge density can be obtained from the y component or the imaginary part of the complex electric field. E that iscomplex electric field is computed as in the Equation 2.27. Using the electric field description with the surface charge density, σ can be calculated from the Equation 2.28.

$$E = \frac{2V_0}{\pi}\frac{y-ix}{x^2+y^2} \tag{2.27}$$

$$\sigma = -4\varepsilon_0\frac{V_0}{\pi}\frac{1}{y} \tag{2.28}$$

From this point, line charge density can be calculated from the integral of surface charge density [62]. Boundaries for the line charge density integral are $\frac{g}{a}$ which is lower limit and g which is upper limit. The lower limit is selected as $\frac{g}{a}$, since to solve the integral the lower limit must be greater than zero, however it must be much more smaller than d.

$$\lambda = -4\varepsilon_0\frac{V_0}{\pi}\log\left(\frac{a^2}{g}\right) \tag{2.29}$$

After the line charge computation, total charge of surface can be found by Equation 2.30.

$$\mathrm{Q} = -4\varepsilon_0 \frac{V_0}{\pi} \log\left(\frac{a^2}{g}\right)(t+w) \tag{2.30}$$

The division of total charge to the potential difference of the surfaces which is $2V_0$ gives the surface capacitance equation for side components of resonator frame.

$$\mathrm{C} = -4\frac{\varepsilon_0}{\pi} \log\left(\frac{a^2}{g}\right)(t+w) \tag{2.31}$$

Surface and gap capacitance expressions can be used to get an idea about dominant capacitance type for the two specified design structures. Pattern of change in capacitance values in a range of dimensions is valued to realize in terms of the effect of design parameters on frequency. Theoretical outputs in this topic might be helpful to be sure about the gap effect on capacitance for the first design structure and specifications.

In Table 2.4, g stands for gap between main splits, g_1 and g_2 exist just for the second resonator design as a small gap dimensions. $C_{surface_1}$ and $C_{surface_2}$ stand for surface capacitance values for first and second designs, and C_{gap_1} and C_{gap_2} represents gap capacitance values just like the surface, they are all in unit of femto farads. Parametric change in capacitance can be realized for all extents of the structures. In this case, other parameters are kept constant and the only change is done on the gap. Width of the frame and splits are *500* μm and one side of the square resonator is *11000* μm.

Dominance between capacitances and the behavior against the varying gap can be observed from graphs of two designs. In Figure 2.16 and Figure 2.17 mentioned relation between capacitances are indicated. In the graph of first design, it can be observed that surface capacitance is above for all values of the gap and for the second design the behavior is the same, except that the amount of the change in gap capacitance is

Table 2.4. Effect of gap on surface and gap capacitances.

g	g_1	g_2	C_{gap1}	C_{gap2}	$C_{surface1}$	$C_{surface2}$
5	1	3	4.04E-14	5.27042E-14	2.13E-13	1.64629E-13
15	6	8	4.02E-14	5.14397E-14	1.82E-13	1.42237E-13
25	11	13	4.01E-14	5.01771E-14	1.67E-13	1.35059E-13
35	16	18	3.99E-14	4.89461E-14	1.58E-13	1.30698E-13
45	21	23	3.98E-14	4.77174E-14	1.51E-13	1.27568E-13
55	26	28	3.96E-14	4.64911E-14	1.46E-13	1.25148E-13
65	31	33	3.95E-14	4.52975E-14	1.41E-13	1.23173E-13
75	36	38	3.94E-14	4.41067E-14	1.37E-13	1.21507E-13
85	41	43	3.92E-14	4.29188E-14	1.34E-13	1.20068E-13
95	46	48	3.91E-14	4.17337E-14	1.31E-13	1.18805E-13
105	51	53	3.90E-14	4.05822E-14	1.28E-13	1.17657E-13
115	56	58	3.88E-14	3.94338E-14	1.26E-13	1.16621E-13
125	61	63	3.87E-14	3.82887E-14	1.24E-13	1.15678E-13
135	66	68	3.86E-14	3.71467E-14	1.22E-13	1.14813E-13
145	71	73	3.85E-14	3.6008E-14	1.20E-13	1.14015E-13
155	76	78	3.84E-14	3.49033E-14	1.18E-13	1.13274E-13
165	81	83	3.83E-14	3.38019E-14	1.16E-13	1.12584E-13
175	86	88	3.82E-14	3.27038E-14	1.15E-13	1.11937E-13
185	91	93	3.80E-14	3.16091E-14	1.14E-13	1.1133E-13
195	96	98	3.79E-14	3.05238E-14	1.12E-13	1.10757E-13
205	101	103	3.78E-14	2.9445E-14	1.11E-13	1.10216E-13
215	106	108	3.77E-14	2.83696E-14	1.10E-13	1.09703E-13

Table 2.4. Effect of gap on surface and gap capacitances. (cont.)

g	g_1	g_2	C_{gap1}	C_{gap2}	$C_{surface1}$	$C_{surface2}$
225	111	113	3.76E-14	2.73065E-14	1.09E-13	1.09215E-13
235	116	118	3.75E-14	2.62412E-14	1.08E-13	1.08751E-13
245	121	123	3.75E-14	2.51908E-14	1.07E-13	1.08308E-13
255	126	128	3.74E-14	2.41411E-14	1.06E-13	1.07885E-13
265	131	133	3.73E-14	2.30977E-14	1.05E-13	1.07479E-13
275	136	138	3.72E-14	2.20685E-14	1.04E-13	1.07091E-13
285	141	143	3.71E-14	2.10324E-14	1.03E-13	1.06717E-13
295	146	148	3.70E-14	2.001E-14	1.02E-13	1.06358E-13
305	151	153	3.69E-14	1.89912E-14	1.02E-13	1.06013E-13
315	156	158	3.68E-14	1.79759E-14	1.01E-13	1.0568E-13
325	161	163	3.68E-14	1.69665E-14	1.00E-13	1.05358E-13
335	166	168	3.67E-14	1.59585E-14	9.94E-14	1.05048E-13
345	171	173	3.66E-14	1.49627E-14	9.87E-14	1.04747E-13
355	176	178	3.65E-14	1.39642E-14	9.81E-14	1.04457E-13
365	181	183	3.64E-14	1.29752E-14	9.74E-14	1.04175E-13
375	186	188	3.64E-14	1.19913E-14	9.68E-14	1.03903E-13
385	191	193	3.63E-14	1.10091E-14	9.63E-14	1.03638E-13
395	196	198	3.62E-14	1.0032E-14	9.57E-14	1.03381E-13
405	201	203	3.61E-14	9.05694E-15	9.52E-14	1.03131E-13
415	206	208	3.61E-14	8.08694E-15	9.46E-14	1.02889E-13
425	211	213	3.60E-14	7.12405E-15	9.41E-14	1.02653E-13
435	216	218	3.59E-14	6.16101E-15	9.36E-14	1.02423E-13
445	221	223	3.59E-14	5.20444E-15	9.31E-14	1.02199E-13
455	226	228	3.58E-14	4.24874E-15	9.27E-14	1.01981E-13

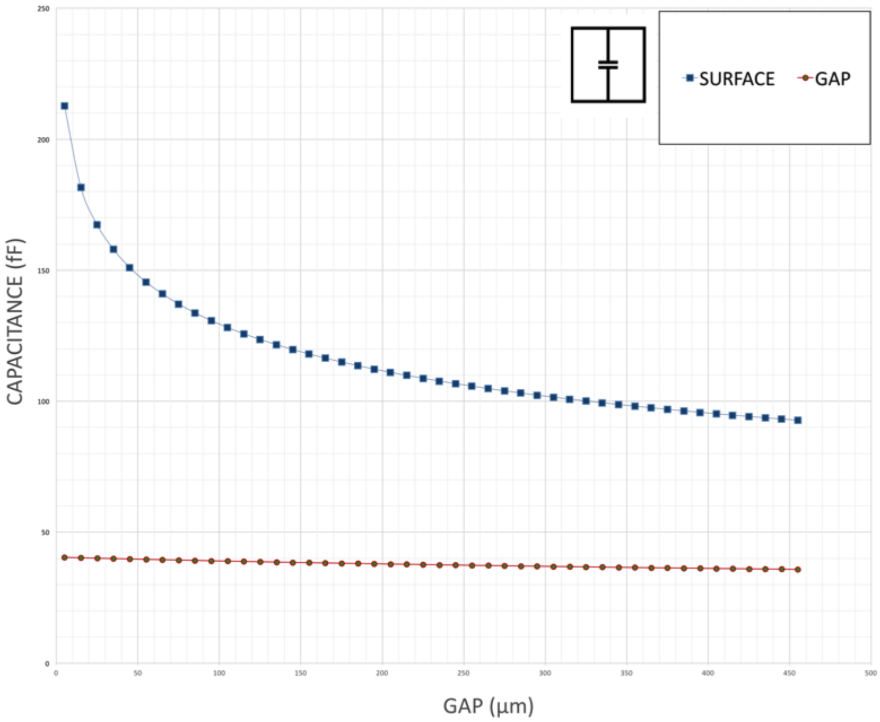

Figure 2.16. Surface and gap capacitance - single gap.

greater.

2.2. Frequency Analysis and CST Simulations

Resonance frequencies of two resonator designs are calculated by hand using capacitance and inductance information previously described. Effect of capacitance change on frequency with increasing split gap is summarized. Calculated frequency can not represent the behavior of device against the current change exactly. At this moment, the calculation is followed by the linear change in gap by number not as a function of mechanically bended cantilever. However, the idea behind capacitance and frequency relation can be realized with this method. Inductance of the square shaped resonator is considered as constant for the sake of simplicity. Besides, as a different resonator structure, resonance frequency of two splits complementary resonator is calculated using real dimensions.

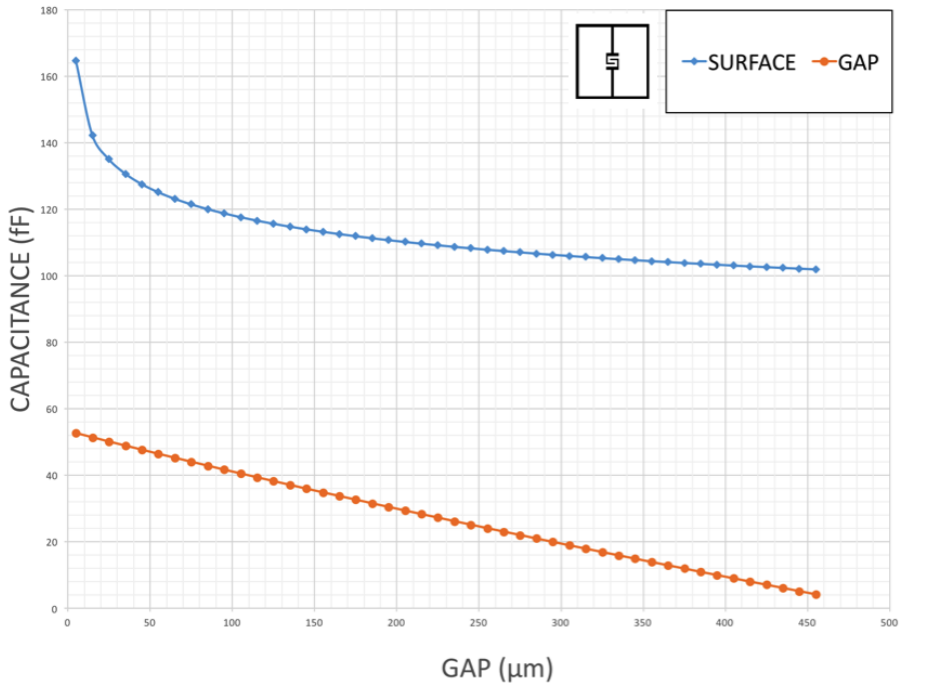

Figure 2.17. Surface and gap capacitance - nested gap.

The tendency can be red from Figure 2.18 and Figure 2.19 for single gap and nested gap resonators. In Table 2.5, calculated values of inductance, capacitance and frequency for real dimensions of three resonator structure are given as SRR-1, SRR-2 and SRR-3, respectively.

Table 2.5. Resonance frequency calculation.

	Inductance (nH)	**Capacitance (fF)**	**Frequency (GHz)**
SRR-1	29.39	138.43	3.529
SRR-2	29.39	125.00	3.713
SRR-3	54.82	68.86	2.587

Frequency analysis of theoretically designed resonators is significant to regulate the design and to be sure that the effect of deposition, release and bending of released structure. Frequency analysis is done with CST Microwave Studio simulation tool

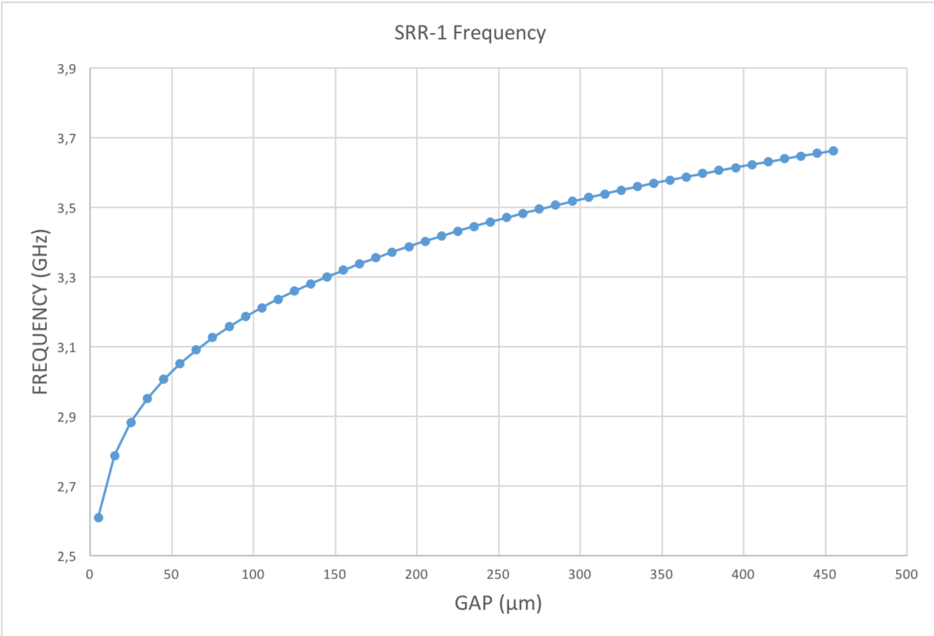

Figure 2.18. Resonance frequency - single gap.

[63].The single split resonator as a fundamental structure has CST simulations for each step of conceiving the device. At first there exist a copper plate on epoxy material just like the printed circuit boards, then the nickel layer is deposited on it, lastly the copper under middle area nickel is etched and nickel is released in this part of the resonator. These three steps are simulated separately and results offer an idea about what we will come across with during the interim steps and final characterization.

In Figure 2.20, simulated S21 parameter of lossy copper layer on FR-4 material is indicated. The resonance frequency is around 3.474 GHz. In Figure 2.21, lossy nickel material is added as a second layer, and as it can be realized the frequency shifts to the higher value, 3.693 GHz.

As a third step, copper under the nickel layer in the middle is removed and nickel is released. S21 parameter simulation, in Figure 2.22 changed resonance frequency is seen as 3.2 GHz. Quality factor is also turned in to a more insufficient value.

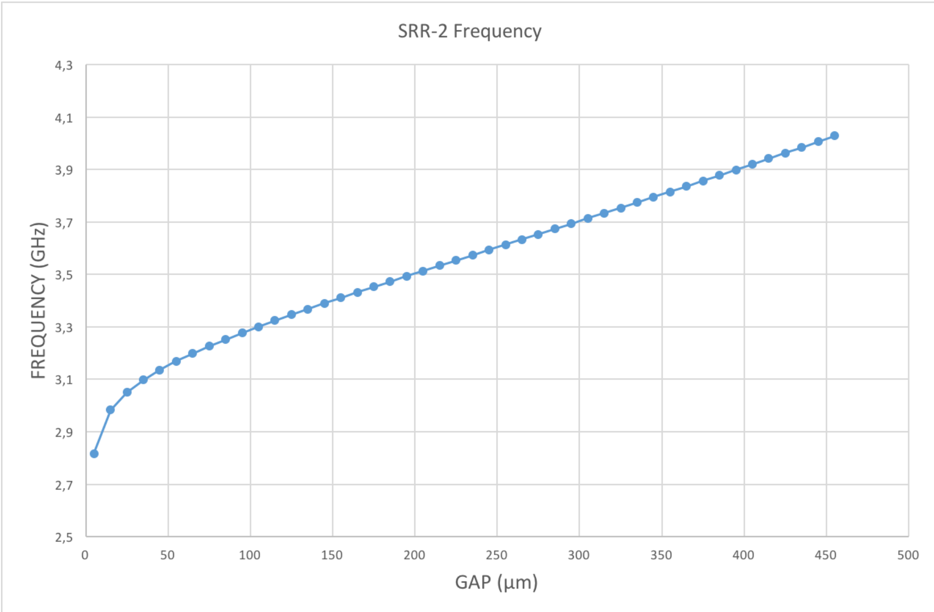

Figure 2.19. Resonance frequency - nested gap.

Lastly, released nickel cantilevers are moved to a six different positions with a bending method. The resulting S21 parameters for six of cantilever positions provide the reference output of varying gap. Tuning mechanism is very similar to this simulation of bending structure, this is shown in Figure 2.23. In the Figure 2.23, there are some values of parameter r which represent the radii of cylinder that cantilevers are bended upon the outside face. The smallest value of the r means the largest bend of cantilevers. Change of frequency is not linear with the amount of the bend, this is because of the nonlinear change in capacitance that is not only comes from the gap but also from the surface. Therefore, the alteration in geometry makes an unexpected change in frequency.

Since the defined simulation limits about the mesh size in the program do not allow, some of the steps in designs as the second one which has a nested gap structure can not be simulated. S21 parameter simulation of the device with only copper layer is given in Figure 2.24. It seems that the resonance frequency is 3.192 GHz. Nickel layer coated resonator simulation for the nested structure is given in Figure 2.25 that the resonance frequency is seen as 3.624 GHz.

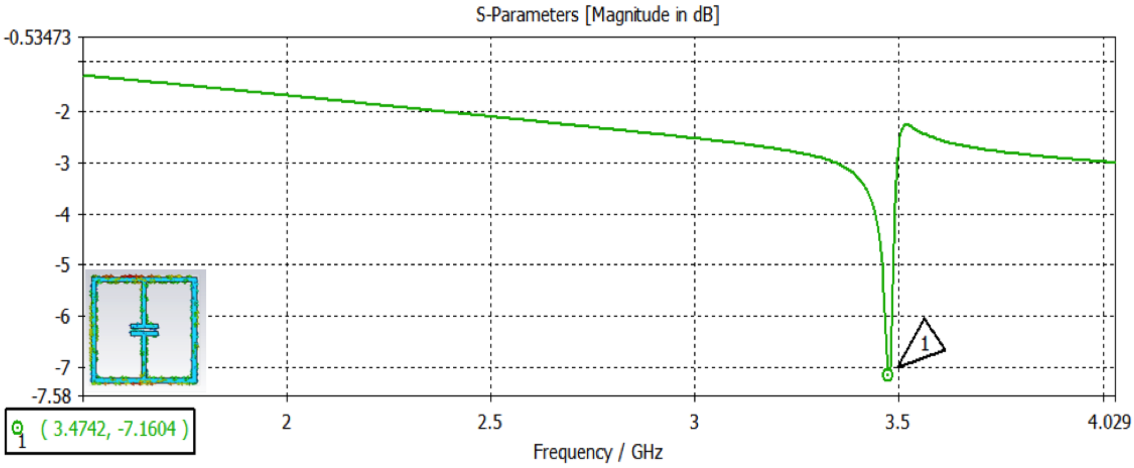

Figure 2.20. S21 of single gap SRR - copper layer.

Other than these, the fifth generation resonators are designed with the help of CST simulations especially to have a reference data before the fabrication of discrete models. In the following four figures from Figure 2.26 to Figure 2.29 S21 response of five designs is illustrated. Designs are shown in Figure 2.8. CST simulation is done for all of the designs but for the first two of them is one simulation is given, because the structure is similar.

Resonance frequencies of designs $(a), (c), (d), (e)$ are nearly 4.0 GHz, 1.4 - 2.7 GHz, 1.45 - 2.7 GHz, and 3.18 GHz respectively. The last design is a complementary version of a commonly used SRR structure [64], and comparing others this design promising.

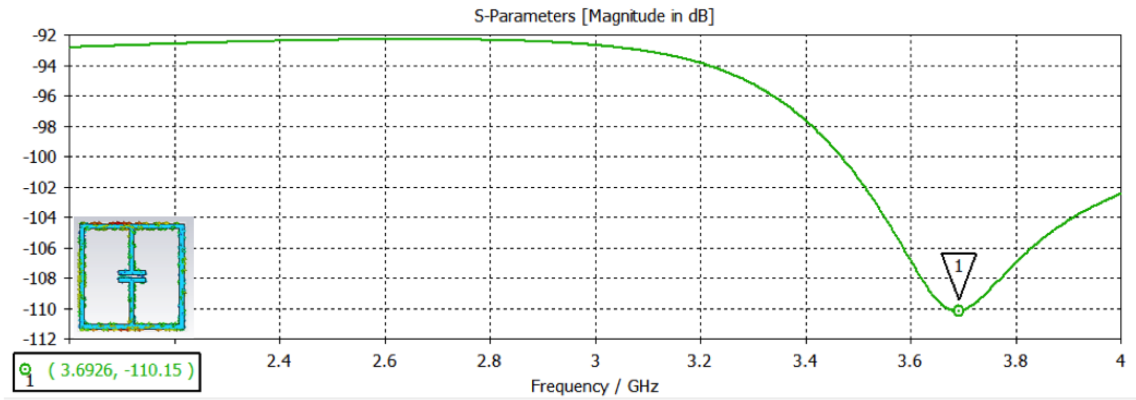

Figure 2.21. S21 of single gap SRR - nickel on copper layer.

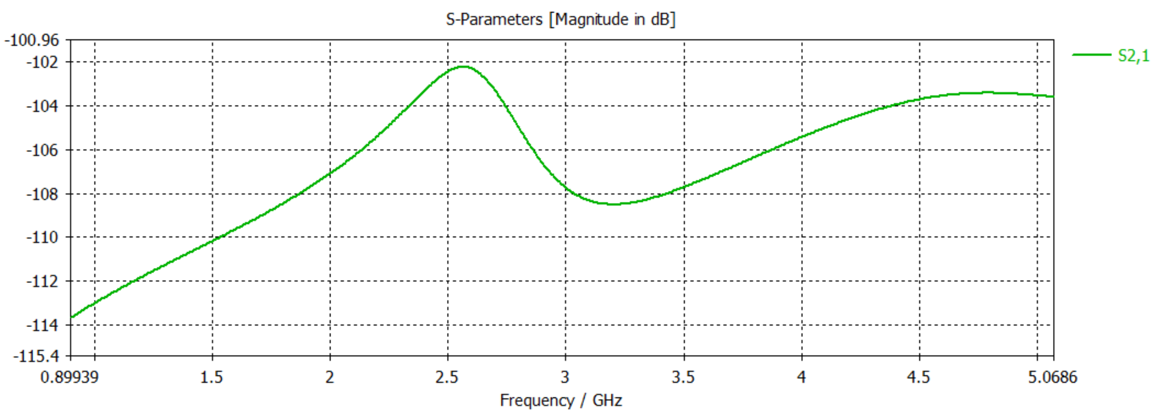

Figure 2.22. S21 of single gap SRR - released nickel layer.

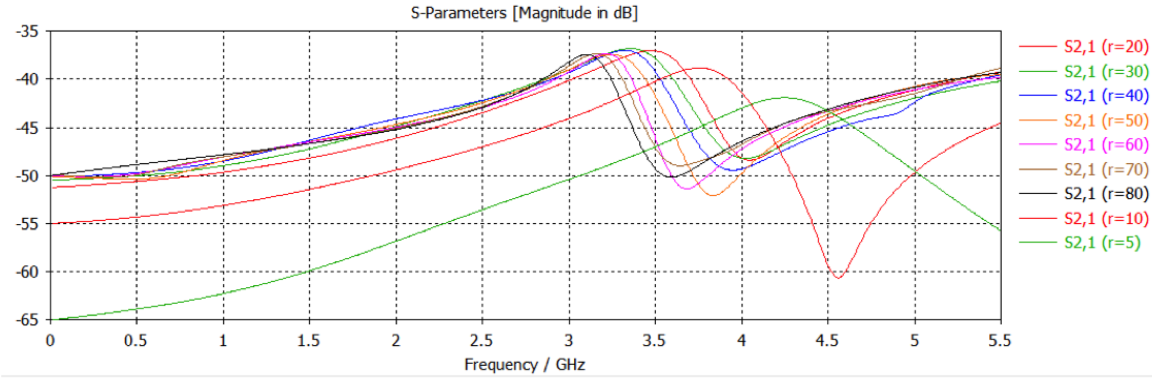

Figure 2.23. S21 of single gap SRR - released nickel layer movement.

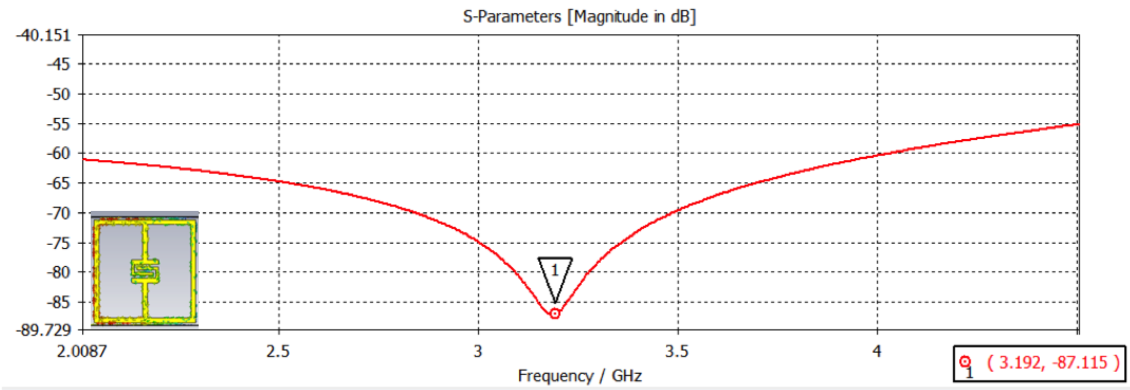

Figure 2.24. S21 of nested gap SRR - copper layer.

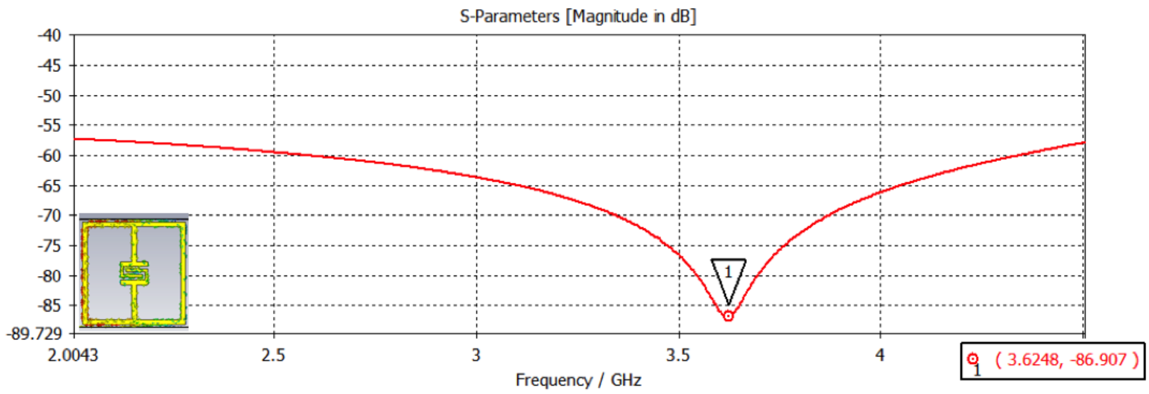

Figure 2.25. S21 of nested gap SRR - nickel on copper layer.

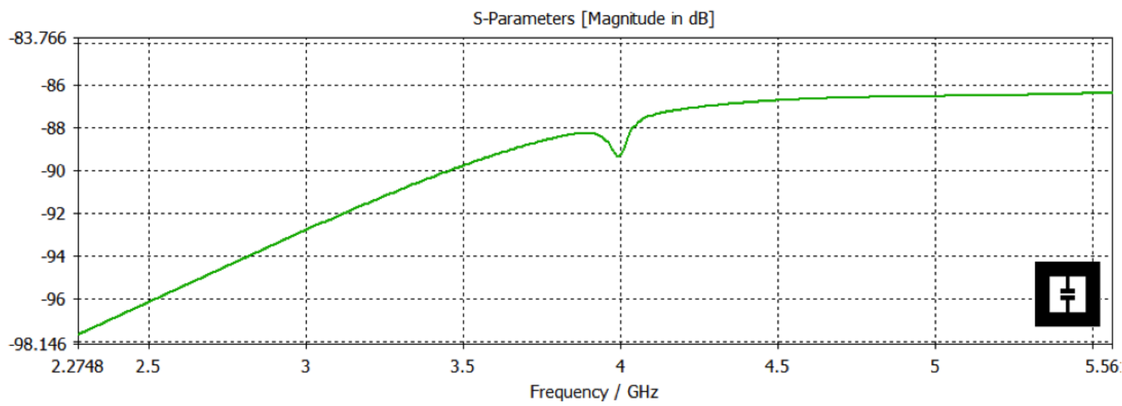

Figure 2.26. S21 of single gap steel resonator-1.

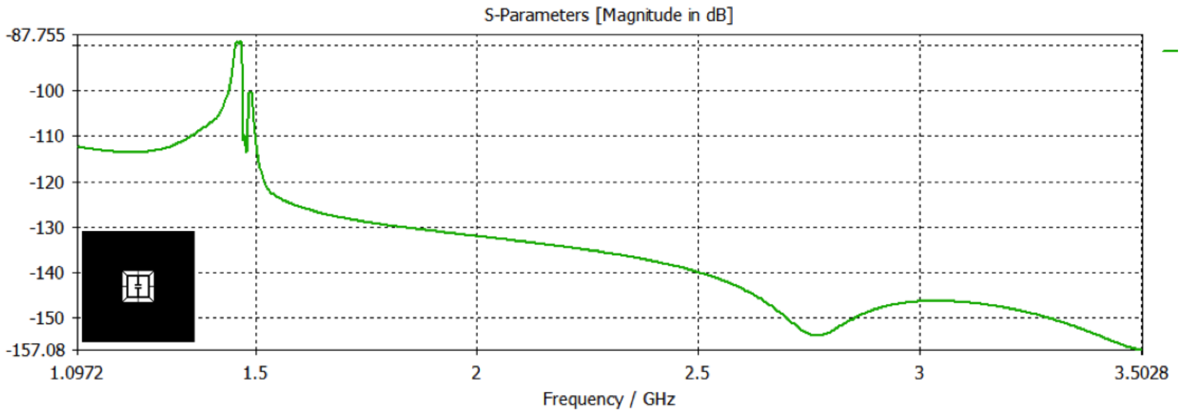

Figure 2.27. S21 of thin anchored single gap steel resonator.

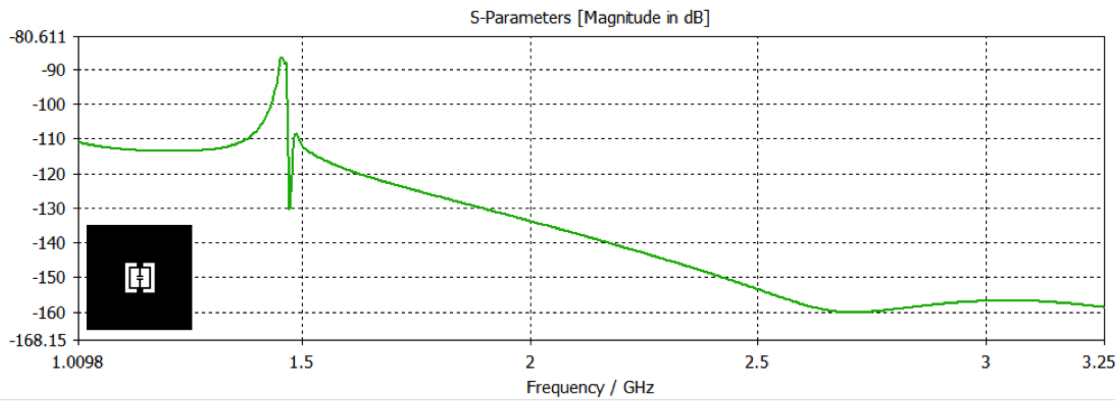

Figure 2.28. S21 of thick anchored single gap steel resonator.

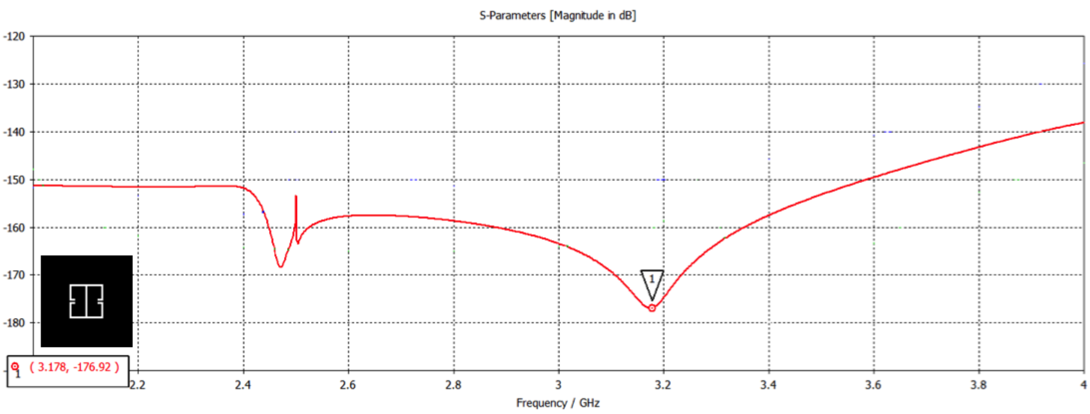

Figure 2.29. S21 of complementary version of two gap steel resonator.

3. FABRICATION

Generated resonators can be divided in to three groups in consideration of fabrication methods. The two basic structure is used for the first generation resonators, which are formed on a one sided copper plate on FR-4 material. Second generation is a different one in terms of general structure, however the eventual resonator is the same as single gap SRR. As a third generation, resonators are fabricated from a steel plate with various modifications on dimensions. For being not complicated, fabrication steps for each of generations will be explained in this chapter separately. Some of the steps are similar between generations, still prominent details are explained on their fabrication.

Initial generation resonators are considered as three bunches due to variations in fabrication steps. There were some problems in fabrication and characterization after fabrication, therefore necessary modifications give birth to new bunches in this generation. In 3.1, these three attempts will be explained in detail.

3.1. Initial Generation Resonators - First Bunch

In the fabrication of the first bunch of initial generation resonators, there are four basic steps. Firstly, resonators are defined on a PCB with FR-4 plate thickness 1.6 mm, and copper layer of 0.035 mm. First step is done to create copper sublayer with a milling - drilling process. At the second step defined structures electroplated with nickel as a second layer that will be released for the purpose of achieve a free-moving cantilevers. A specific part of the resonator must be released, therefore the other part is shielded with photoresist. Photolithography step is performed using a properly designed mask. Covered part of the design is the main frame of the resonator. Lastly, a selective etchant is used to release the uncovered nickel layer by etching the copper under nickel selectively.

3.1.1. Milling - Drilling Resonators on Printed Circuit Board

The first layer of the resonators are created with milling and drilling process on a PCB. Two specific designs mentioned before are drawn in Eagle PCB design software. Resonators take form as an array with the circuit board plotter machine. Figured resonators are uploaded to Circuit Pro PM program in Gerber format, milling and drilling options are selected on that software that is used in LPKF branded PCB manufacturing machine in our laboratory. The reason for using such a machine for the first layer instead of classical PCB manufacturing methods is to obtain the structure complete in better precision and also getting many of them to make five to ten trials. A strict and precise sublayer helps to realize better second layer during the fabrication.

3.1.2. Nickel Electroplating

Electroplating is widely used technique especially in industrial application for nickel, silver, copper and zinc plating of metals. In microelectronic fabrication, electroplating is not used very often because of the lack of information about its thickness. Critically small thicknesses might be uncontrollable, however an elaborated plating bath with a careful control of current provide foreknowledge about the thickness. If advanced measurement methods are also considered, the nickel device fabricated with electroplating can be convenient to study.

The formation of a movable structure on the copper plate requires the deposition of a thick metal film. Because of the significant effect of the thickness and ductility on the quality of tuning, other metal deposition techniques fall behind the electroplating method. Besides, nickel electroplating is an inexpensive and smooth way to achieve low stress, ductile and conformal coating [65].

Physical embodiment of electroplating consists of anode that is in this case a nickel ingot, cathode is the resonator device that we will coat with the nickel, the hydrated electrolyte solution and a power supply gives the required current, the schematic of the electroplating setup is shown in Figure 3.1. Hydrated liquid is specific conductive

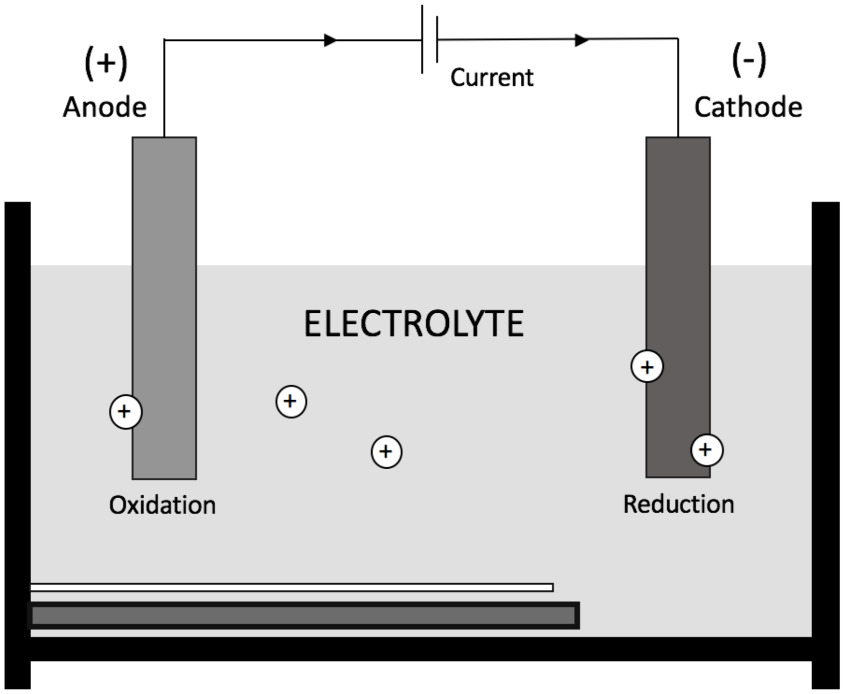

Figure 3.1. Representative schematic of electroplating bath.

solution for the anode metal. Applied current is carried by this conductive solution with the help of oxidized metal ions.

The process can be described as follows; when the power supply is connected to the anode and cathode, the current begins to flow through the connection and the electrolyte. At this time, metal ions on the anode surface become oxidized and leave the surface. Oxidized metal ions itinerate in liquid media until they meet the cathode surface. Electrons on negatively charged cathode surface set the positively charged nickel ions free. On the cathode surface, metal ions are reduced and they take their places on the surface as free metal atoms. Concurrently, the remaining negative ions turn out to be discharged with positively charged anode [66, 67].

<u>3.1.2.1. Electroplating Bath Setup.</u> Attributes of electroplating bath is one of the most significant issues to take into account during the electroplating process. Bath

is composed of 1 cm thick polypropylene material that is designed to study with acids. Inner dimensions of the bath are 15 cm, 30cm, and 25 cm width, length and depth respectively. The volume of the solution with a 3 cm safety space at the top is nearly 10.5 liters. Heating of the solution is done via a quartz heater placed at the bottom. There exist also a thermocouple temperature sensor in another quartz tube beside the heater.

The heater and thermocouple is connected to the control unit through two holes. Spaces around holes were occluded with a separate polypropylene and additional glue against leakage. A water proof silicon liquid seal is coated as another precaution. The purpose of the control unit is to be sure about the temperature and also to arrange it to the required value with high precision, that is in this case 0.1 °C. The bath and the control unit is shown in Figure 3.2.

3.1.2.2. Quality Improvement of Electroplating. There are some critical points need to be rigorous to raise the quality of plating. Every effect on surface can disrupt the plated metal layer. Composition of the electrolyte must be in its ideal state, because water molecules and other polar molecules behave like dipoles during the process. After a metal layer is formed on the cathode surface, some of positively charged ions attract these dipoles and generates aqueous molecules on the cathode surface. These molecules forms a thin layer called as cathode diffusion layer on the surface. Cathode diffusion layer prevents the metal ions sent from the anode to be reduced and plating gets harder [68].

Manifestly, to obtain better plating quality, cathode diffusion layer thickness must be reduced as possible. Temperature of the electrolyte should be kept at its proper value, the decrease in temperature causes the increase in layer. Current density is also a factor such that the increasing current density decreases the layer thickness. Enhancement in metal ion concentration affect the layer negatively. Agitation of the solution is another point to consider, because the higher the agitation speed the lower the layer thickness. Lastly contamination of kinds of salts can assist the layer thickness, therefore it is need to be careful about contamination.

Other than cathode diffusion layer, agitation is significant to ensure homogeneous temperature and concentration across the entire solution. Current density should be kept at a proper level, it must be high for cathode diffusion layer, however if the current density is much higher than it must be than there will be excessive hydrogen gas release on cathode surface originated from reduced cations. Overmuch release induces low quality porous plating [69]. In our work, we need bright, ductile and thick nickel layer, therefore the temperature, current density and pH of the solution as well as the purity of the surface of the cathode sample are all crucial.

3.1.2.3. Electroplating Process. In the first instance, the plating bath is prepared by bleaching with DI water for 8 hours. Then, it is bleached with 60 g/l trisodiumphosphate solution at 50 °C for 8 hours. As a last step, $5 - 10\%$ $H_2\ SO_4$ solution is put to the bath and bleached at 60 °C for 8 hours. The bath is rinsed a few times and dried with the nitrogen gun.

The bath is filled with the electrolyte solution that is a commercial product of Enthone, with name LECTRONIC 10-03 HSX. Solution is sulphamate based. This electrolyte solution provides the ductile, low stress, bright nickel electroplating. As it is mentioned before, the solution is agitated with a magnetic stirrer by the rotation of paramagnetic fish inside the solution. The speed of the rotation is more than 1000 rpm. In the beginning of the process, to prevent the unsteady motion of fish, rotation speed is set to a lower value as 400 rpm. The speed is increased with time before the plating process. The pH value of the solution is 3.7 as desired. The bath composition and optimum values of other auxiliary parameters are listed in Table 3.1.

In the plating process, contact regions of anode and cathode should be kept away from the solution. Additionally, a holder is needed to carry heavy nickel ingot of 12 cm x 10.5 cm x 1.5 cm volume without any damage to the contact area. Other than these, we had to be careful about the contamination to the bath, regrettably the nickel

Table 3.1. Bath Composition.

Nickel Metal	113 $\frac{g}{l}$
Boric Acid	40 $\frac{g}{l}$
LECTRONIC 10-03 Anode Activator	85 $\frac{g}{l}$
LECTRONIC 10-03 HSL Addition Agent	22 $\frac{g}{l}$
LECTRONIC 10-03 Wetting Agent	10 $\frac{g}{l}$
Temperature	58 °C
pH	3.5

ingot itself seems dirty even though it is pure nickel.

Firstly, the nickel ingot is cleaned with 2.5 % $H_2\ SO_4$ solution and DI water for 30 minutes. A holder is designed and prepared from a kind of polymer material which can act also as a filter. The holder is hanged to the bar on top of the electroplating bath. The bar is bonded between two sides of the bath via spaces exist there. The filter ensures the low contamination, easy way of holding the ingot and keeping contacts above from the solution. Isolation bands are used on contacts and the filter holder is cleaned as the ingot itself.

As a first step copper samples with 2.5 x 2.5 cm area are plated, the quality of the plating, and the deposition rate is observed. Current is around 100 mA and plating process is done for 10 minutes for all samples. In every two minutes, samples are weighed to calculate the plating thickness. Current - voltage value, current density for copper samples is given in Table 3.2 and in Table 3.3, plating time and average thicknesses of samples are listed.

Resonators are plated with the same procedure, cathode contacts are established via thin isolated cables that are soldered gingerly to corners of resonators.

Table 3.2. Parameters of sample electroplating.

	Current (mA)	**Voltage (V)**	**Current Density ($\frac{\mathbf{mA}}{\mathbf{cm^2}}$)**
1	313	1.94	7.4
2	271	1.93	7.5
3	209	2.0	21.0
4	308	2.55	38.5

In the first bunch of initial generation resonators, the thickness of plated nickel could not be known exactly, however the thickness is calculated from the product of deposition rate and plating time, as a nearest estimation method . Samples are plated for 12 minutes with nearly 0.2 $\frac{\mu m}{min}$ as the rate of deposition, therefore the thickness is around 2.4 μm.

Deposition rate is calculated by the following procedure, a copper sample that has a known area is weighted with isolation bands just before the plating process and after plating the sample is weighted again using a precision scales. Hence, plated thickness is calculated with difference of two weights, the area knowledge and the density of the nickel metal.

Table 3.3. Resulting thicknesses of sample electroplating.

	Plating Time (min)	**Average Thickness (μm)**
1	2	0.45
2	4	0.95
3	6	1.35
4	10	2.15

3.1.3. Lithography

In the lithography step, we want to preserve the frame of the resonators that the etchant of the next releasing step can not damage the frame. The uncoated area is the middle of the structure, meanly cantilevers that will be released. Lithography step is significant to give desired form to device by the etching process.

Theoretically, lithography is the process of producing patterns on the material. Coating is done with a liquid polymeric material called as photoresist. Photoresist is sensitive to ultraviolet light so that exposed or unexposed areas become soluble in a solvent named developer depending on its type as negative or positive. The photoactive compound in resist makes this formation possible by changing to a carboxylic acid on exposure to UV light in the range of 350 - 450nm. Carboxylic acid is soluble in developer solution, so that the exposed areas become soluble. In defining the exposure areas a mask is used, for this reason the structure is cardinally depends on the exposure and mask [70].

Firstly, the mask was designed and printed in high resolution printer to prevent small blanks. The mask was drawn in L-Edit drawing program. Dimensionally, the dark frame was designed wider than the covered layer, this is because of the fact that the etchant can damage the coated layer because of its anisotropic etching characteristic. After dimensional control with a sample paper printing, mask was printed on a transparent thin flat plate. Mask can be printed on a glass film as it is used in usual, however for our process conditions the mask film is used in soft contact with the sample.

It is required to mention about sample cleaning process, because the layer must be well cleaned before to spread the photoresist that is so sensitive about the particles. Particles can stay under the photoresist and prevent the develop process of features must be patterned. Sample cleaning procedure is as follows, the sample is washed with first acetone, then DI water. Secondly, isopropanol and DI water is used to wash. Then for 5 seconds it is kept in 1:100 sulphuric acid and washed with DI water. Lastly, 1:100 hydrofluoric acid is used for 5 seconds and final wash. Mask is also cleaned with isopropanol and washed with DI water before the UV exposure.

Preliminarily, TI Prime is coated with 4000 rpm speed of spinner for 40 seconds. The sample is baked 2 minutes on a hot plate with 120 °C and let it to cool. The next step is the PR coating, the thickness is decided as 2 μm. AZ5214 PR is used after centering the sample. This was a problematic process, because the sample is not a silicon wafer, dimensions and therefore the vacuum capability of the spinner was not enough. After some trials, it is spin coated for 40 seconds at 4000 rpm speed. Durability of the PR in the etchant depends on baking process beside all other coating process details. Temperature of the hot plate is reduced to 110 °C, then the sample is baked for 50 seconds.

Prepared sample is exposed to UV with 40 $\frac{mJ}{cm2}$. The humidity in the laboratory is highly effective for lithography process [71]. To prevent undesired effects such bubbling, it is required to wait for ten minutes before and after the UV exposure step of the process. In the end, the sample is ready to develop features. For this purpose, AZ400K developer is used with 1:4 (developer: DI water) concentration. Patterns was seen after about 75 seconds of waiting time, for the clear defining extra 5 minutes is waited. After this step, another hard bake process can be done, if the coming next process is wet etching.

3.1.4. Wet Etching - Releasing

Etching is an essential process in micro-fabrication of integrated circuits, MEMS and other micro buildings [72]. Patterns of layers that construct the whole device come to existence with etch process. Etching can be done with two basic methods, first is wet etching and the second is dry etching. In wet etching processes, the sample is etched with the proper solution at a convenient temperature. Dry etching is basically achieved with the help of powered gas plasma. There are several mechanisms of using the plasma in a chamber at appropriate pressure, RF power, gas flow and gas mixture. The main difference between the two processes is about their etching style. Anisotropic etch can be achieved with some of dry etching mechanisms is very desirable in some steps of micro-fabrication if the feature size is too small to stay in the isotropic nature of the wet etching.

Isotropic etching nature of wet etchants can be asked for a releasing process, because the under layer can be etched away with only the etchant can move under the top layer. Wet etching process can undermine the top layer if the top layer is not soluble in the etchant. In our releasing step we take the advantage of this theory behind the etching process, as representative Figure 3.3.

Process conditions has great importance in etching process. As it is mentioned before, temperature of the etchant must be well arranged at the proper value. In general, acids are used in wet ething steps of micro-fabrication and temperature dependency of the etch rate of such solution is critically high. Even for 0.5 °C, etch rate can change about 50 $\frac{nm}{min}$. As a second parameter, agitation during process can be counted. In general, agitation rises the etch rate. Any contamination in to the etchant can disrupt the process, because some particles can stick on the sample and behave like photoresist, therefore the etchant and the container must be quite clean. Lastly, while working with chemicals, proper gloves and a protective mask have to be used, safety comes first.

Etchant of this process must be highly selective for copper and nickel metals. Selectivity of an etchant can be considered as the ratio of the etch rates of specified layers are exposed to etching process. In our releasing process, the uncoated top layer must be stay solid and the under layer copper must be etched away. Nickel compatible etchant consists of glacial acetic acid : 30 % hydrogen peroxide : DI water in 1 : 1 : 18 by volume [73]. At 20 °C, etchant temperature , etch rate is about 500 $\frac{nm}{min}$ for the copper layer that is deposited with metal sputtering method. In our case, copper layer is already exist on FR-4 material with a different adhesive strength.

The thickness of the copper layer on FR-4 material is about 35 μm, and the longest way under the nickel layer that the etchant has to deal with is 250 μm. In consideration of the etch rate, the removal of the copper layer takes a long time as 8.5 hours.

In the process, first the sample was cleaned with isopropanol. Ultrasonic vibration is used to increase the etch rate. After about 60 minutes, etched areas appeared slowly, in 75^{th} minutes, much of uncoated area is etched. The etch rate can be calculated as 470 $\frac{nm}{min}$ from this process. Unfortunately, copper under nickel layer did not dissolved during following 3 hours. Layer is controlled in microscope seemed to as it did not allow to etchant go through under layer. Because, the copper layer is defined in the very first step and sidewalls of the copper layer is also coated with the nickel that rejects to act with the selective etchant.

The actual problem about the process was the endurance of the photoresist. 2 hours later, photoresist became distorted and little hollows are formed on coated area. Frame of the resonator is destroyed and process did not continue.

3.2. Initial Generation Resonators - Second Bunch

The flow of fabrication process for the second bunch of resonators were redesigned to eliminate the releasing problem that we came across with the first bunch. Instead of etching with milling and drilling process we used to define the first layer we let the copper layer stay as it was. In the first instance, a photolithography process for defining the area to be nickel electroplated is considered. After the developing process of lithography, the resonator shaped area is prepared for the nickel electroplating as just we did before for the first bunch of resonators. Firstly, nickel is plated on the desired copper spaces, the resist is stripped of, then the third step is followed with second lithography. In the second photolithography step, it is aimed to cover the area of that will not be released in the last step. Lastly, the copper layer is intended to be released with selective wet etching process.

The difference between first bunch and the second bunch of resonator generation is to assist the wet etchant that can go nickel layer underneath without causing that much deformation of resist and coated layer.

3.2.1. First Lithography

The mask of the first lithography step is designed and drawn in L-Edit program. The design mainly consists of two resonators with two monopole antennas for each of resonators that is used to characterize the resonance frequency with a network analyzer. Additionally, there are dummy structures that will help to decrease the current density, and alignment marks for the aligning process of the second mask of second lithography process. In Figure 3.4 the mask is shown, as in the first bunch, masks are printed with the high resolution printer so that the tiny spaces can lead to destroy of the photoresist.

The process was very similar to the 3.1.3. First of all, the sample and the mask are cleaned with acetone to get rid of the finger prints, organic particulates and other oil included contamination that can grow during preparation of the sample that is around 4 inch by diameter. Isopropyl alcohol is used to clean the substrate and the mask more.

At the beginning of the process, the sample is coated with TI Prime in the coating spinner with 5000 rpm speed for 50 seconds. The purpose of covering the sample with TI Prime is to promote adhesion of resist to the substrate. In other case, adhesion can be not enough to protect the under layer during the electroplating process. TI Prime coated sample is baked at 120 °C for 2 minutes. The positive photoresist AZ5214 is coated in spin speed 4000 rpm for 40 seconds. Hot plate is cooled down to 110 °C and post-bake process is done for 50 seconds. The sample is exposed to UV light with the first mask on. Contact printing method is used in all lithography steps because it is reasonable to have a contact between mask and the sample in our possibilities. Developer solution AZ400K is prepared as 1:4 with DI water. The sample is agitated for 40 seconds in the solution.

3.2.2. Nickel Electroplating

Necessary regions of the sample is protected with the photoresist and sample is cleaned with isopropyl alcohol for 30 seconds. Two points are selected on dummy spaces on the sample to connect the cathode cables. Thin copper cables are bonded with soldering.

Electroplating bath is prepared by cleaning it with 60 °C hot DI water for 8 hours, and washing for a few times with cool DI water. Electrolyte solution and the recipe of preparation was the same as in 3.1.2.3. The bath is heated up to 58 °C with 400 to 800 rpm agitation by the help of magnetic fish in the bath and magnetic stirrer. The speed is significant to provide controlled agitation, therefore it begins with 400 and during the plating process it is risen up to 800 rpm. Nickel ingot is cleaned with sulfuric acid and washed with DI water for 5 minutes.

At this time the difference is that the sample is coated with the photoresist. Therefore we should have controlled the reaction of photoresist against the electrolyte solution even if we checked it from literature. A photoresist coated piece of sample is steeped in the electrolyte solution in a test beaker. Then, durability of the photoresist and change in its surface is controlled, there was no problem. In normal conditions, the photoresist can not be solved in nickel electrolyte solution and it can be stiff up to 300 °C.

As a conditioning and controlling step, some copper and brass pieces are electroplated and the current is set to 50 mA first and 100 mA for the next. Current density was about 14 $\frac{mA}{cm^2}$. Our sample is deposited for 20 minutes, in every 4 minutes sample is controlled. After the deposition is finished, a clear, bright and very adhesive nickel layer came to existence. Deposited thickness could not be measured exactly, because of the accuracy of the precision scales that might provide the only estimation about the thickness.

3.2.3. Second Lithography

Second lithography process is done for the purpose of covering necessary areas that will not be solved in the etchant solution. Before the new photoresist is laid on, the previous one is cleaned with the acetone, right after with the isopropyl alcohol. The sample is coated with the TI Prime as in the first lithography process after cleaning and drying process is completed. Pre-bake process is done at 120 °C temperature for 2 minutes on the hot plate. As we experienced the perishability of the photoresist in our previous study, we decided to coat the sample with another photoresist named as AZ4533. 4000 rpm speed of spinner for 40 seconds was adequate to obtain a thicker photoresist. The measured thickness of the photoresist was around 5 μm. Post-bake process was at 110 °C for 1 minutes.

The critical part of the exposure step was the alignment of the two layers. After the mask cleaning process, alignment marks are controlled carefully with the optical microscope, the mask and the sample is contacted. UV exposure is given in dose of 40 $\frac{mJ}{cm2}$, and features are developed in the developer solution. The picture of the sample finished with the second lithography step is shown in Figure 3.5.

3.2.4. Releasing

Nickel compatible copper etchant is prepared. The temperature of the solution is measured as 17 °C. The exact etch rate of the solution have not be known before the process, however after some copper is etched it is calculated by the measurement of the remaining thickness. The etch rate is around 770 nm per minute. The thickness of the copper on the FR-4 substrate is around 35000 nm and the width of the cantilever is 1 mm, therefore the process must have been 5 hours 30 minutes long according to the estimation.

Wet etching process is done with agitation by hand for 3 hours, in every 15 minutes the layer is controlled and in each passing 30 minutes the solution is prepared over again. There was a clear etch in copper layer, however process can not be continued for remaining 2 and a half past hours, because of the reason that the photoresist became punctured and the structure have been damaged. A picture of the sample in wet etching process is shown in Figure 3.6.

3.3. Initial Generation Resonators - Third Bunch

Second bunch of initial generation resonator fabrication was unsuccessful due to the releasing failure. Therefore, we concentrated on the releasing step, and we changed the design slightly. The intellectualized study about the structure is that if resonators are modified with dimensionally necessary and sufficient holes on the part that will be released, the copper layer can be etched away uncomplicatedly. Process steps are kept unchanged. First step is a lithography step that forms the coverage for nickel electroplating. Second step is nickel electroplating, third is again a lithography step and lastly the releasing process is processed with wet etching.

3.3.1. First Lithography

The importance of lithography process is experienced during the first and the second bunches of initial generation of resonators. The mask have to be very clean and well printed; because, due to the effect of the acidic solution, distorted or inconveniently covered areas become erroneous processed. Printing of masks were a troublesome study, since to figure out a professionally printed mask or the printer equipment was not available.

The first mask is redesigned and drawn in L-Edit program, immediately after it has been printed. The first mask is exhibited in Figure 3.7 with some magnification.

Photolithography for the first layer have been processed attentively. Steps have been done as in the 3.2.1. Positive photoresist is coated with 4000 rpm for 40 seconds after the cleaning and TI Prime coating steps. Following the pre-bake step, the sample is connected to the mask and UV light applied as 40 $\frac{mJ}{cm2}$. Developer solution is prepared and in 50 seconds all of the features come into existence. Lastly the post-bake process is executed.

3.3.2. Nickel Electroplating

Electroplating is a novel method that makes perfect depositions on even a micron feature size in structures. The design is developed to a new one that has little square spaces, which have been protected in the photolithography step. Uncovered areas are dimensionally small, however as it is mentioned, in a careful electroplating process these features can be deposited easily.

First the electroplating bath is cleaned with DI rinsing and dry. Solution is agitated during the temperature rise up to 58 °C. At this time, connection cables are connected by soldering the empty dummy structures. Sample has been electroplated for 24 minutes with 100 mA current. The current density is about 15 $\frac{mA}{cm^2}$. The plated thickness of the sample could be measured precisely for this time by the help of the profile meter device in the clean room. The thickness of the electroplated nickel is about 4.2 μm. In the Figure of 3.8, some pictures of the nickel electroplated sample are demonstrated. Additionally, in Figure 3.9 microscope images of the sample is given to show electroplating of thin spaces on cantilever parts.

This was not really enough for the released structure excitation because there should be thicker and manageable layer that can move linear in excitation. However, to obtain thicker nickel layer can be achievable with the two following; first increasing the time which can lead to removal of photoresist, and the second is that if we increase the current density which can promote the deposition rate, the deposition will be darker and porous. The dark surface affects the measurement step and porous nickel layer has low elasticity that is the crucial point in working principle of the device.

3.3.3. Second Lithography

Second lithography is considered as the most critical part among all other fabrication steps because we had disappointing experiences from the previous generations.

Photoresist must be adhesive, thick and well defined to obstruct the corruption in the protected regions of the structure. The reason of the deteriorated structure tried to be eliminated by recreating the mask. Unfortunately, a new printed one also had some gaps can be seen with a hundred times magnification. There can be other methods could be applied to improve the endurance of the photoresist, however clean room facilities are not adequate. Additionally, a high quality mask printing is not possible in our situation.

Process steps were as in the following, first TI Prime is coated and sample is baked on the hot plate. AZ4533 photoresist is spin coated and baked for 50 minutes at 110 °C. Lastly, the mask and the sample is aligned, UV exposure is given and photoresist is developed in AZ400K and DI water developer solution. Second photoresist layer as developed is indicated in Figure 3.10.

3.3.4. Releasing

As it is displayed, sample copper piece included four resonator structure together, and before releasing step resonators are separated. A guillotine is used to separate the heated sample in purpose of preventing crack or any other damage. Nickel compatible copper etchant is prepared for the releasing step. 1:1:18 Acetic acid : Hydrogen Peroxide : DI water included etchant is agitated for 30 seconds, and first piece of the sample is put into the beaker. After 35 minutes, uncovered nickel cantilevers are left from the copper layer that have not been etched in an observable way. The separated nickels are broken off in a minute and the sample has gone.

The solution is prepared carefully for the next experimental study. The temperature of the solution is measured as 21 °C, and that is a clear temperature for the etchant and the sample. The etch rate is controlled, it is also as it is expected from the previous studies. A dummy copper piece is put into the etchant to observe the chemical interaction. These all check procedure is done before another trial.

In the etch process of the second sample, after 20 minutes passed the nickel parts are raveled out and became shattered in seconds. As a result, the etch rate of the copper is not high enough to catch up the speed of nickel leaving. Nickel Layer is expected to be more adhesive to copper layer. In addition, another observation about the adhesion is that the nickel layer must be more sticky in itself. The reason of the failure could be the poor deposition, and also could be the guillotine cut. During the separation process, guillotine applies a considerable pressure on the sample that might be above of the stress and elasticity boundary.

3.4. Second Generation Resonator

Resonator structures designed to obtained voltage controlled oscillator device are considered as movable split cantilevers included makings. It is observed that the critical step in fabrication of these type of devices is the releasing. It is assumed that if the device is fabricated as released stem from itself, deposited layer the subject of magnetic excitation could be bended with the movable stem. For this purpose, a structure is designed and drawn in SolidWorks 2015 program as a three dimensional body can be seen in Figure 3.11.

3.4.1. 3D Printing

In design, resonator has the same dimensions with the previous generations. Columns resonator settled on are thinner than the frame width of the resonator to support the resonator without being coated in sputter machine. Additionally, the two monopole antenna is designed on both sides of the resonator. A square piece is added to the upper side of the resonator to connect the cathode cables during the electroplating process avoiding any damage on the resonator itself. Merger line of square piece and the resonator is designed as thinner than the resonator, therefore after the electroplating process is completed, the piece could be separated from the resonator to be characterized.

Deviation, linear-dimension and angle tolerance controllable 3D printer device can be utilized to print structures in stereolithography format. Various materials can be used in printing. In this design, we need a soft material with good elasticity, because we need to have effortless movement in the structure. In clean room laboratory, tango plus material was exist as a fine elastomer [74] and the structure is printed with tango plus material. During printing, the structure is covered with a soft simple support material. Support material has to be cleared off to continue with the device process. 1% solution of sodium hydroxide solution is employed to remove support material. Completely clean structure is achieved after 20 minutes soak process of sodium hydroxide. Unfortunately, at the end of process, the structure become divided into two pieces. Resonator was sturdy, half of the column was broken. Resonator body is bonded to a thin FR-4 plate to emplace the sample on the stage in the sputter machine properly.

3.4.2. Metal Deposition with Sputtering

Metal layer deposition on an elastomer material is achieved with sputtering technique which is explained both in [75, 76]. The purpose of deposition of a metal layer is to form a seed layer for nickel electroplating process. Magnetron sputtering machine is available in clean room laboratory and that can be processed without any deformation in sample. Supplied current, pressure, and target material properties are principal parameters in deposition. DC/RF magnetron sputtering machine is indicated in Figure 3.12

A base layer for electroplating process could be titanium and gold depending on material availability, for this time gold is selected. An additional layer under selected metal layer is needed in this process, because of adhesion problem in tango plus material. Chromium is used to promote the adhesion of metal layer. The deposited chromium thickness is 20 nm. Gold layer is about 250 nm. Indeed, for a well defined metal layer could make study faultless can be achieved by processing various materials for a few times, however the sample printing takes much time. Therefore, a well known material is selected relying on experimental studies performed previously.

Sputtering process is handled successfully, however the plate under resonator is also deposited with the metal. A gold etchant is used to clean undesired sides. A picture of the gold-chromium deposited sample can be seen in Figure 3.13.

3.4.3. Nickel Electroplating

The substructure for the nickel electroplating is prepared with metal sputtering. Cathode cable connected to the contact point by soldering after sample cleaning. Electroplating bath is cleaned and prepared. Temperature of the electrolyte solution is 58 °C and pH is 3.7 that the solution is proper for the material of the sample. Electroplating process is done for 26 minutes in control. A bright nickel layer is formed on the gold-chromium coated sample. Even if the sample material is compatible with the electrolyte solution, adhesion of metal layers to the sample can be affected by the temperature and current passing so that the plating time is considered as sufficient.

3.5. Third Generation Resonators

The resonator manufactured with steel material is one of our studies in purpose of obtaining a structure has cantilevers independent from the sublayer. Magnetic excitation of an independent structure is easier, because the releasing process is complicated to handle with current facilities. The most affecting part of this study is that, steel is a perfect material to shape and move. Steel is a magnetically excitable material depending on its composition that means there is no need to coat the resonator any other magnetic layer. As another advantage of utilizing steel material in the study is the bright surface of the steel. In characterization, good reflection of the light from the steel surface can make the measurement of deflection possible.

There exist several types of steel material depending on its fabrication and composition. In this study, stainless steel material is selected. Stainless steel type basically covers various corrosion resistant steel materials. Chromium percent in the composition affects the corrosion resistance. Mechanic, magnetic and electrical properties changes depending on other elements included, such as nickel. Nickel compound features magnetization, so the type can be called as ferritic steel.

Processed resonator samples can be recognized from Figure 3.14. There are two samples of resonators shown with a difference, one of them has screw holes to connect it to a different resonator holder.

Stainless steel plate with 0.4 mm thickness is used in this fabrication. Resonator design is drawn in SolidWorks 2015 program and saved in .DXF format. A laser cutter machine compatible with metal plate shaping exists in laboratory is employed to cut the plate according to the designed structure. Laser cutting precision is about 300 μm. Resonator samples are cut, and dimensions of the sample are the same compared to the design. As an effect of laser cutting process, there are some burn marks on the front sides of features, however both sides of the resonator can be used to characterization.

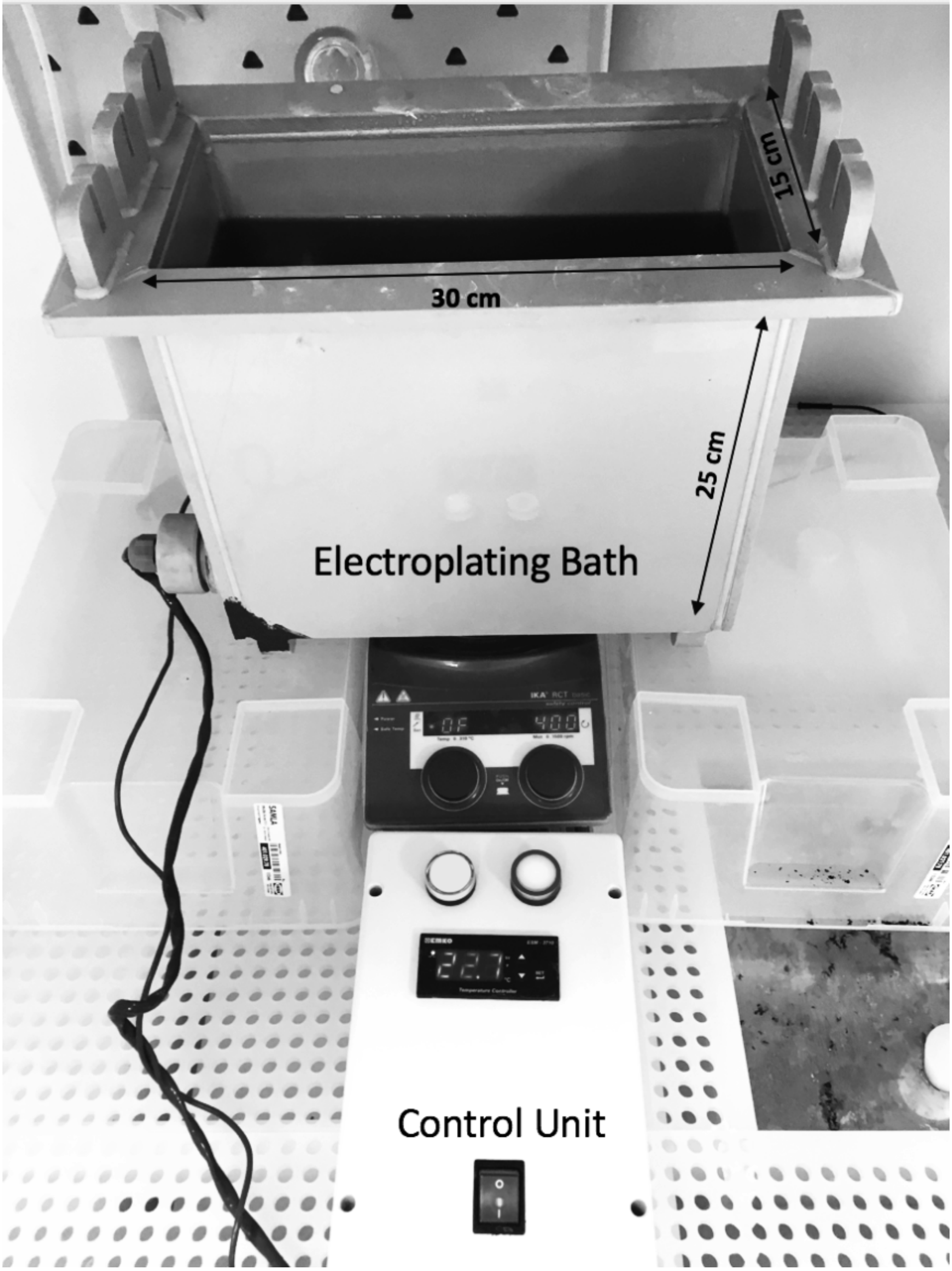

Figure 3.2. Electroplating bath and control unit.

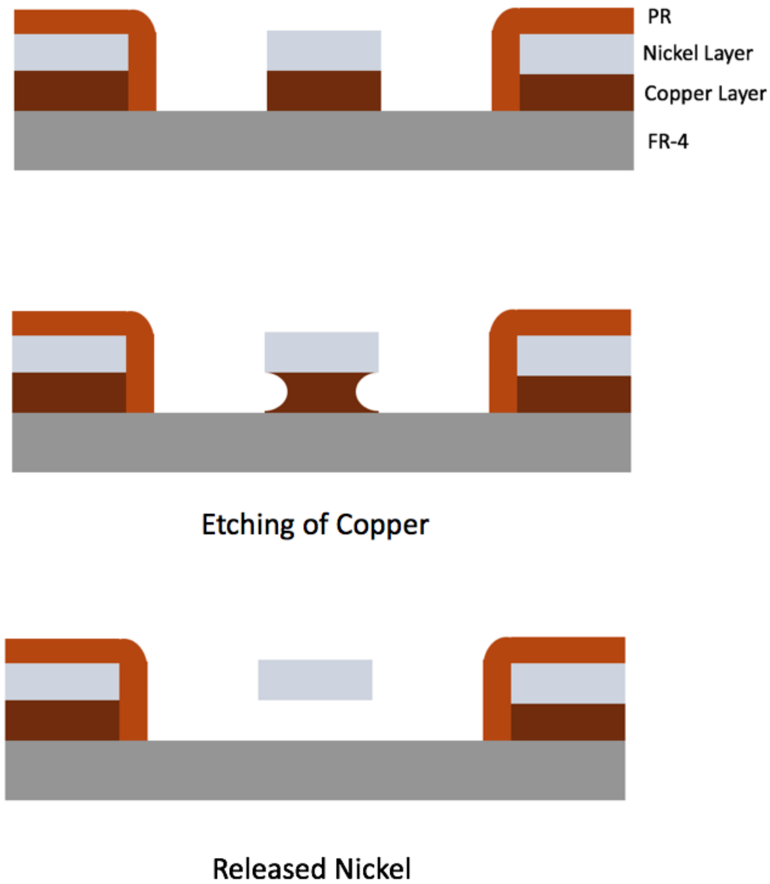

Figure 3.3. Under etch and nickel releasing.

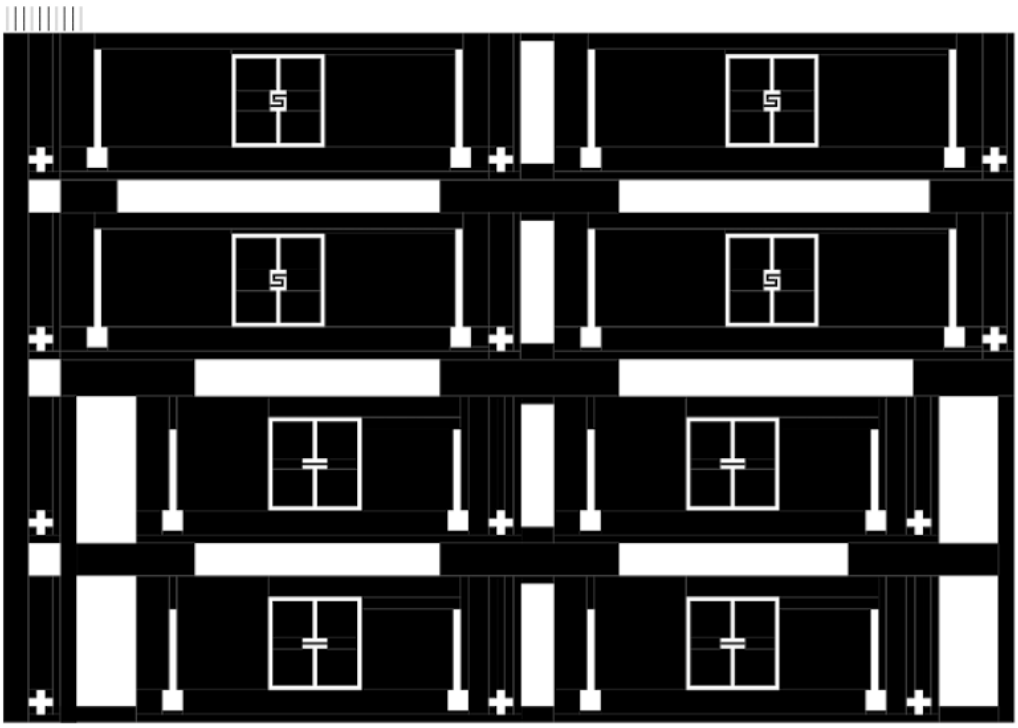

Figure 3.4. 2^{nd} bunch - mask for the first photolithography step.

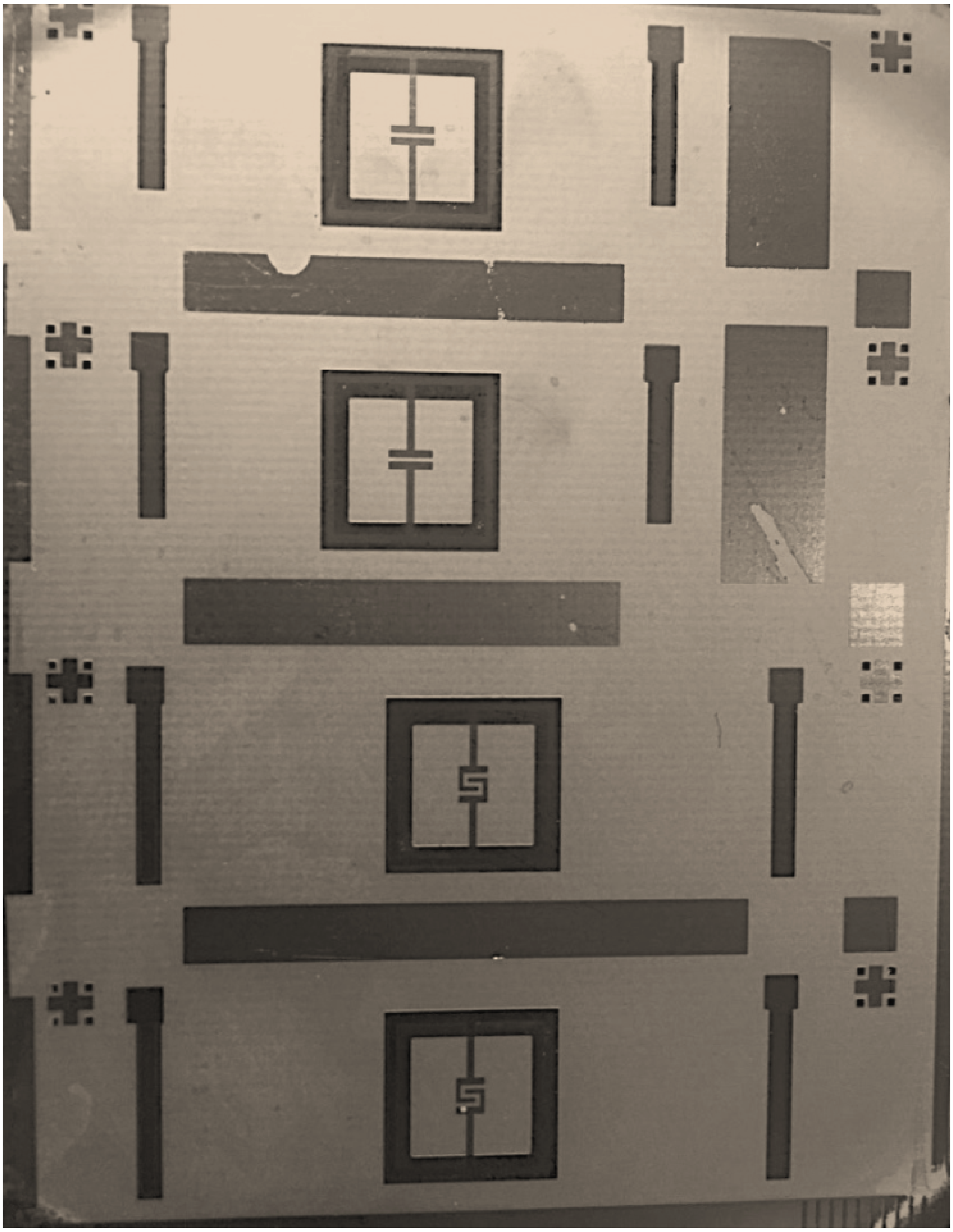

Figure 3.5. 2^{nd} bunch - the sample after second lithography process.

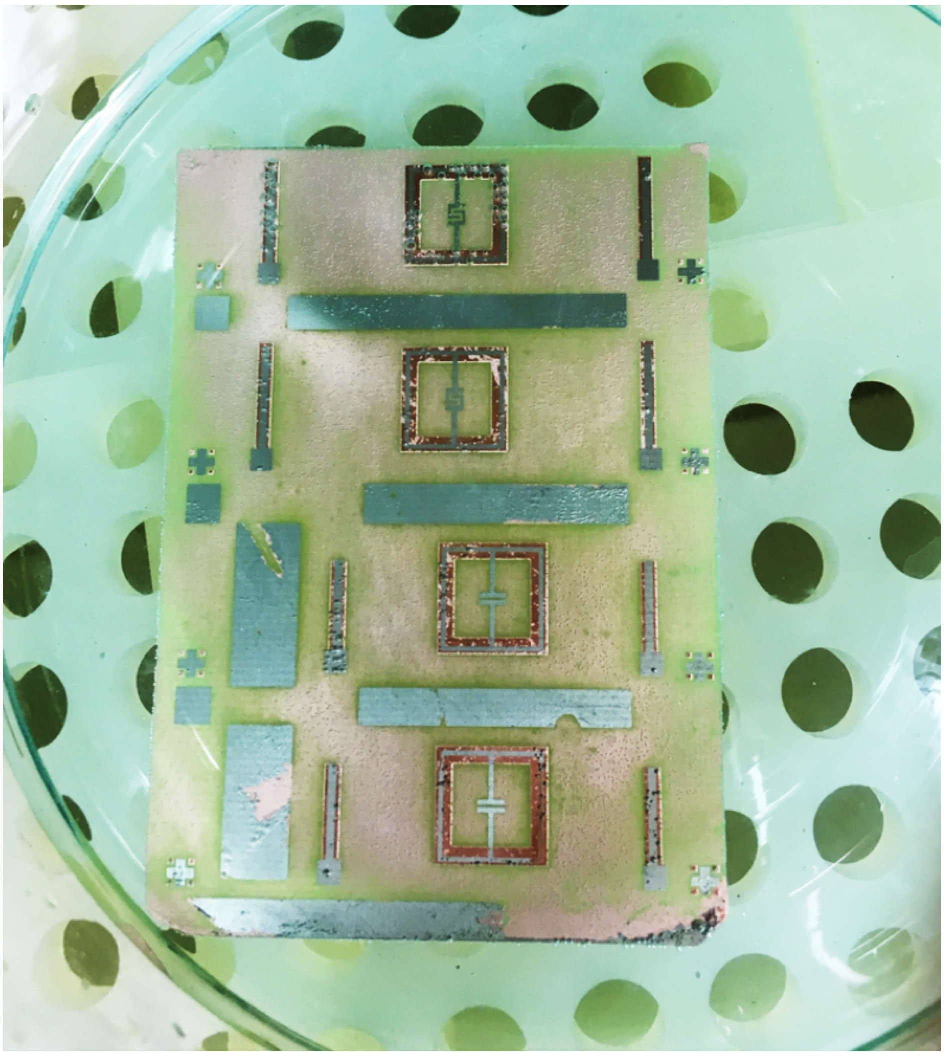

Figure 3.6. 2^{nd} bunch - the sample during wet etching process.

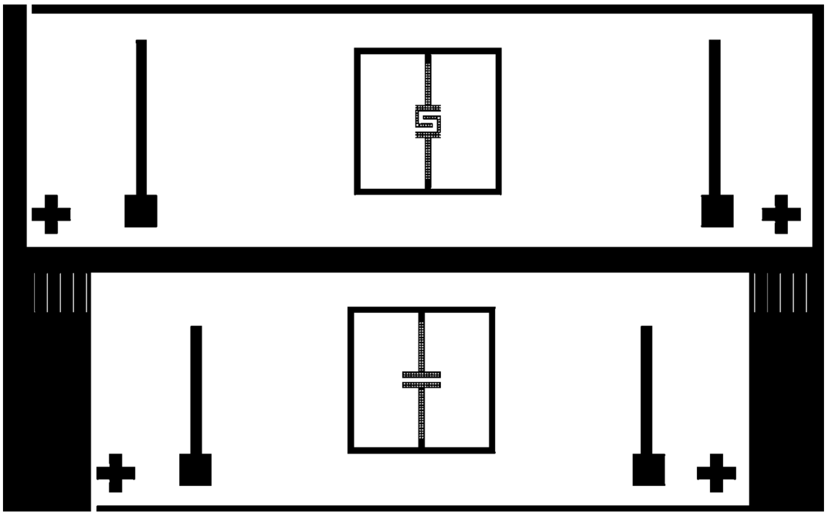

Figure 3.7. 3^{rd} bunch mask for the first photolithography step.

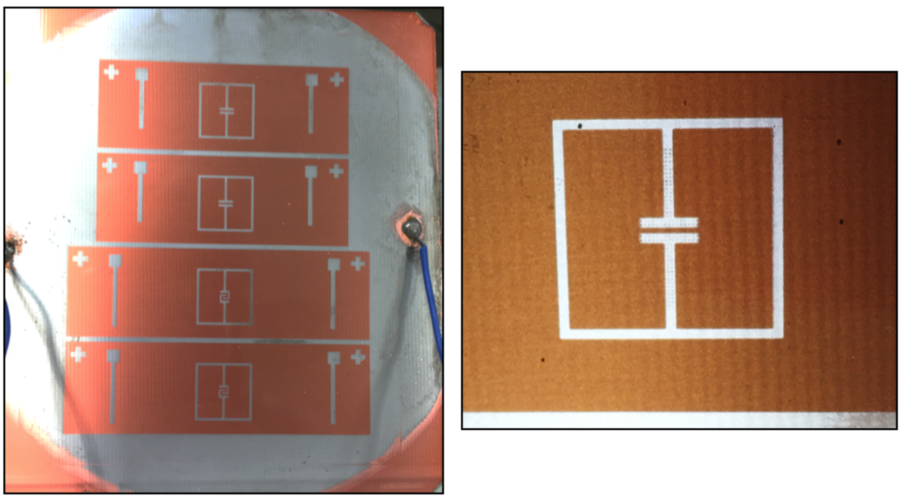

Figure 3.8. 3^{rd} bunch - pictures of nickel electroplated sample.

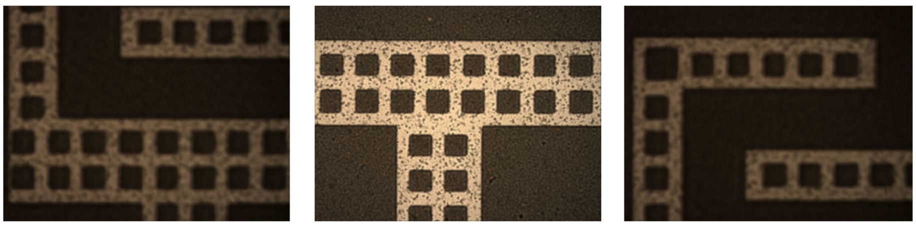

Figure 3.9. 3^{rd} bunch - microscope images of nickel electroplated sample.

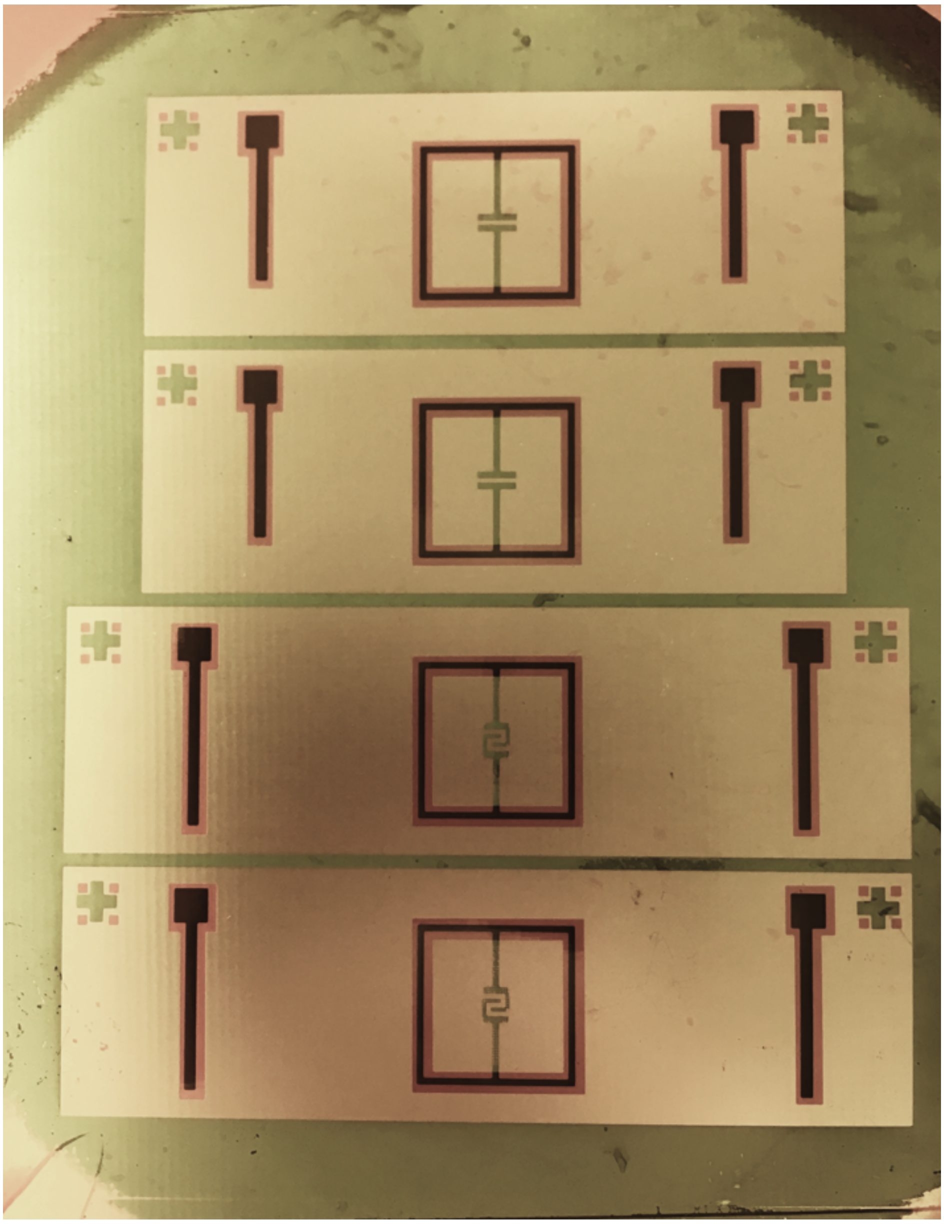

Figure 3.10. 3^{rd} bunch - second photoresist layer on nickel electroplated sample.

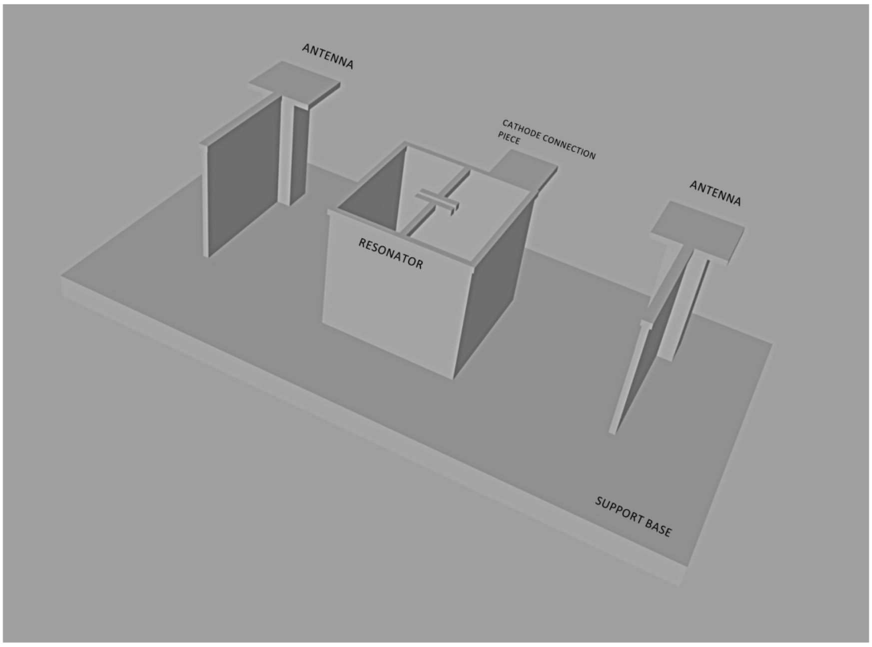

Figure 3.11. Three dimensionally generated resonator.

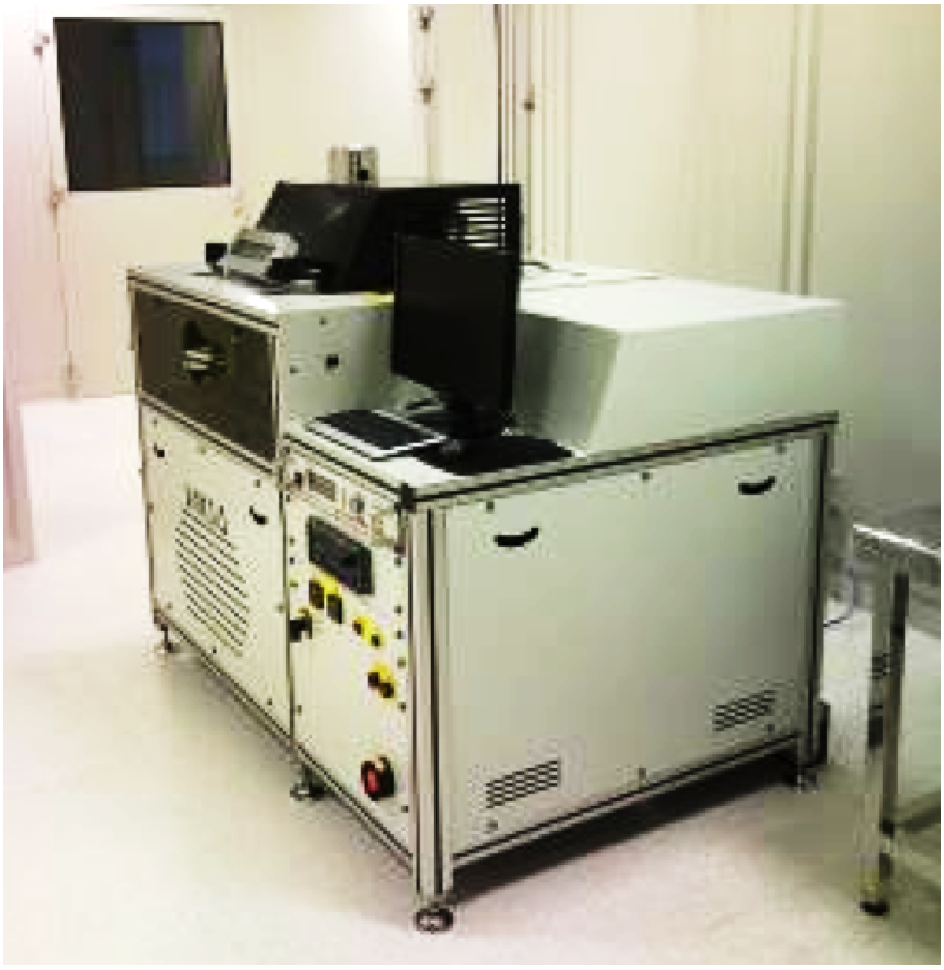

Figure 3.12. DC/RF magnetron sputtering machine.

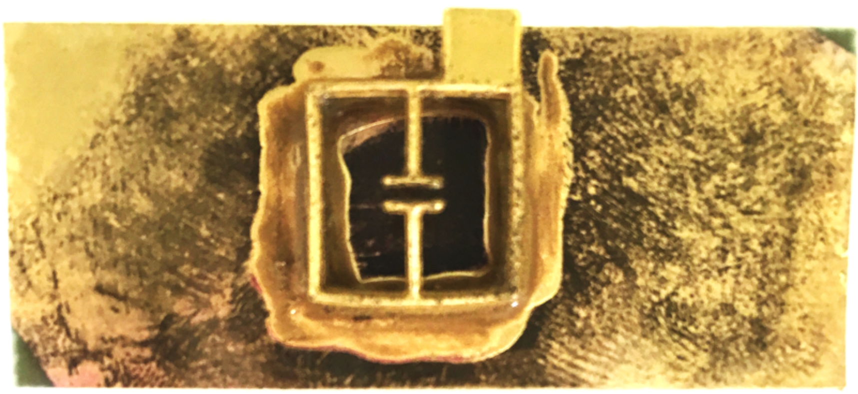

Figure 3.13. 3D generated resonator sample after metal deposition with sputtering.

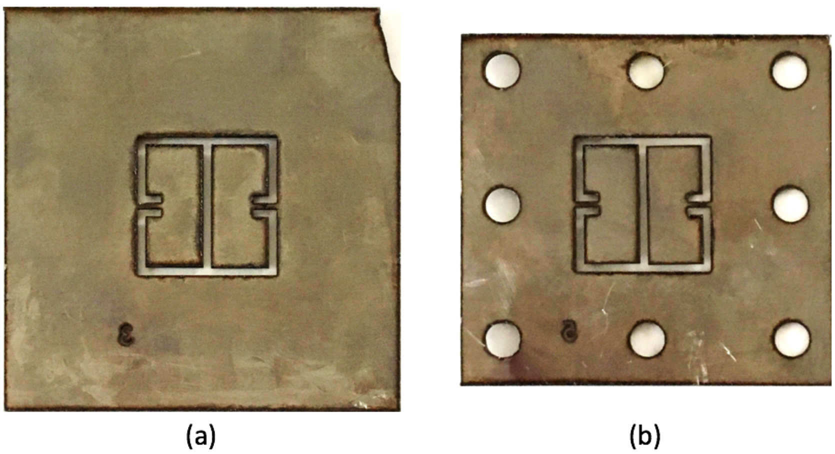

Figure 3.14. Stainless steel resonator samples. (a) without screw holes. (b) with screw holes.

4. MEASUREMENT AND CHARACTERIZATION

Characterization study is significant as much as other steps. It is possible to count resonators are working voltage controlled oscillator circuit elements only if their frequency response and mechanic behavior is as it is expected. Measurement setup has great importance on findings, and also on creating a reasonable study about fabricated device. Resonators' responses are studied to form a meaningful output by characterizing them according to theoretical assumptions.

In this chapter, measurement and characterization study of fabricated resonators are discussed. Theoretical background of measurement, detailed explanation of measurement setup and measurement results are expressed respectively.

4.1. Theoretical Background and Measurement Setup

Observation of resonance frequency of resonators is the first step in measurement procedure. Resonance frequency can be extracted from the measurement of S-parameters. S21 measurement gives the resonance frequency of the resonator placed between two monopole antennas connected the two ports of network analyzer [12, 23]. Monopole antennas are designed according to the resonators' estimated frequency range.

Implementation of magnetic force to the cantilevers is another critical issue in measurement. Magnetic force can be applied in different ways, however the main point is to be able to change the amount of applied force in an observable manner. A magnetic coil driven by direct current can effectuate the necessary magnetic force that can be arranged by the amount of driven current. A current carrying loop conductor creates a magnetic field in direction found by right hand rule. Amount of created magnetic force and its direction is related with the magnetic field formed by the relation given in Equation 4.1. In the relation, force is affected by two parameters, first is the number of turns, second is the change of the magnetic flux with the time [77].

$$\mathbf{F} = -\mathbf{N}\frac{\Delta\Phi}{\Delta t} \tag{4.1}$$

In consideration of the amount of force, number of turns of the coil can not be controlled because in the study commercially available electro coils are used. There is only thing that could be played with is the magnetic flux which is responsible for the magnetic field created. Magnetic flux is directly proportional to the magnetic field, therefore magnetic field can be altered. Magnetic field of a electro coil can be found by the formula given in Equation 4.2. As it can be seen in the equation, magnetic field depends on number of turns, length of the coil, current passing through the wire and the permeability. The only parameter that can be played with is the current. Electro coil is operated in DC mode. AC mode is also applicable for some applications, however in characterization of resonators in this study, applying direct current is conceived.

$$\mathbf{F} = \mu\frac{N}{l}\mathbf{I} \tag{4.2}$$

Another important point is to decide the amount of displacement of cantilever beam when the exciting force is applied to the end portion of the cantilever. Cantilever acts as a spring attached from one side. Displacement under magnetic force can not be seen by naked eye, estimated measure of movement was around 10 μm. Observation of the amount of displacement can be achieved by a humble reflection method using a laser light source.

In steady state, laser light is reflected to some point on a scale board. Next, excited and moved end portion of the cantilever changes the hit position of the light. The difference on the scale board can be measured easier, therefore the angle of movement and displacement of the cantilever can be extracted from the reflection law of rotating mirror. If the rotation angle of the mirror is θ then the deflection of the reflected light will be 2θ. Using the geometrical relation between angle and the length seen on

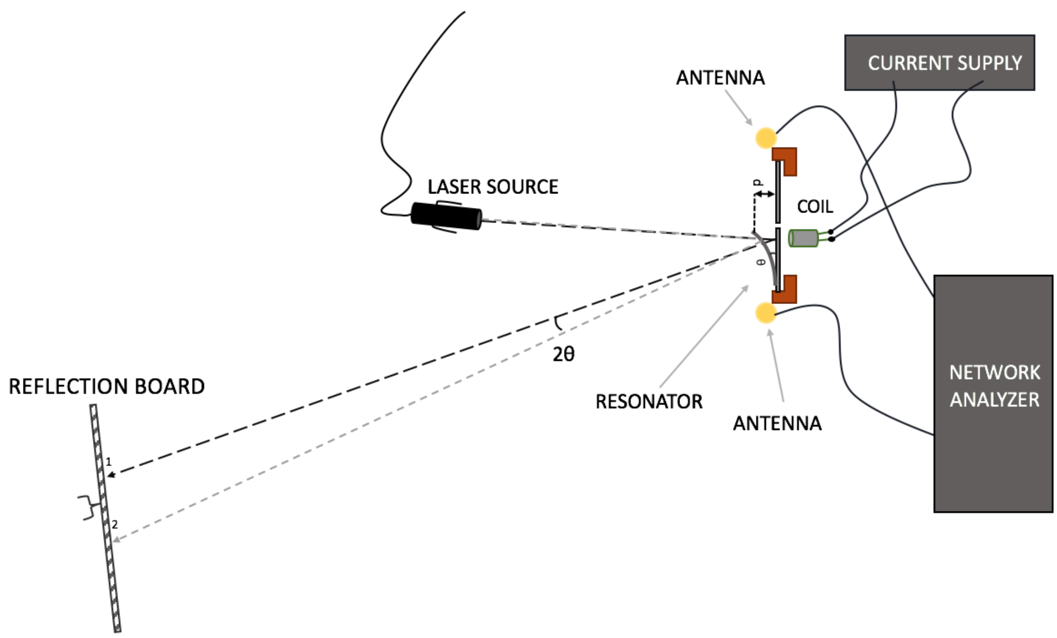

Figure 4.1. Representative measurement setup.

the reflected plate, deflection angle of the mirror can be found, so that the amount of displacement also can be featured. Representation of the measurement setup can be seen in Figure 4.1.

Characterization method have to be combined with a well designed and properly established measurement setup. Resonator, supply devices and other tools have to be insistent enough to eliminate environmental diversions.

Resonance frequency of initially generated resonators was measured in steady state with and without nickel plating. Because there is no characterizable device in terms of tuning frequency, measurement is just left as a one step.

3D printed device was tried to be measured as it is explained theoretically, however during the experiment, some part of the metal layer on device is lifted off and after that one of the cantilevers was broken. Even these misfortunes, there is some results representing the steady state and under constant magnetic force of magnets. Picture displayed in Figure 4.2 belongs to the measurement setup of the initial generation

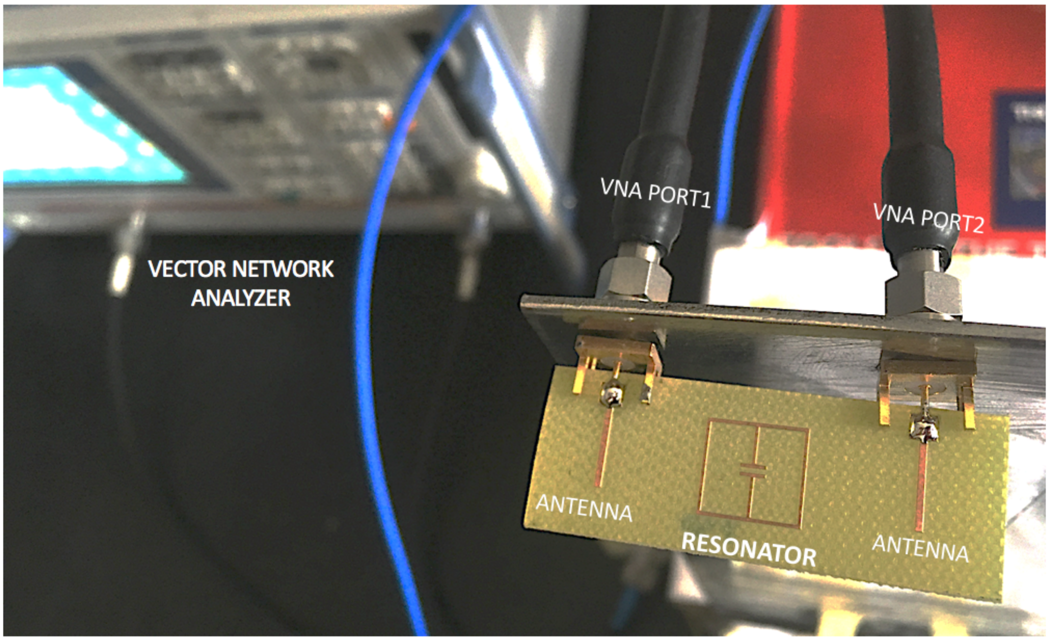

Figure 4.2. Initial generation resonator measurement.

resonators.

Measurement study of steel resonators is successful. Devices are set up on a stabilizer table using fixing rods. Resonator is fixed with a rod connectable tool designed according to the dimensions of the resonator. Two monopole antennas are made from a thick copper wire. Network analyzer and antennas are connected and fixed properly behind the resonator. Laser source is placed at 50 cm away from the resonator. Reflection board is placed behind the laser source and the distance between resonator and the board is 240 cm. To keep the light spot and prevent scattering some optical lenses are used.

Improving the reflectivity of the resonator surface one pieces of gold coated silicon is pasted. In addition, magnetic dipole moment of the resonator is strengthened with six pieces of tiny magnets. These can effect the measurement result, however when it has been checked the amount of change that they create, it was not that significant. To take a picture from measurement setup was difficult, so that there is a picture of some part of measurement setup shown in Figure 4.3. Due to some reasons laser source

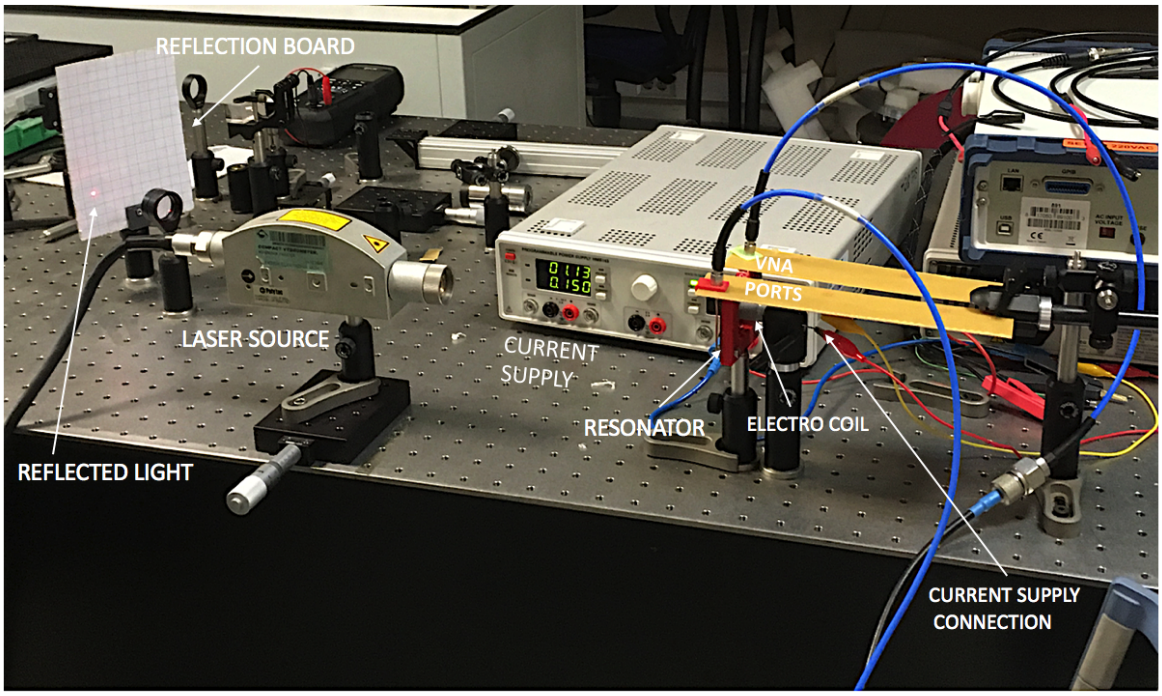

Figure 4.3. Measurement setup-1.

is changed in last two measurement study. In Figure 4.4, fixed steel resonator and magnets on it are exhibited.

4.2. Characterization

In this section, characterization of generated devices will be explained. As in the fabrication section, according to their structural characters, results will be given in separate subsections. In subsection 4.2.1, results of initial generation resonator structures is summarized. In subsection 4.2.2, 3D printed device measurement results and lastly in subsection 4.2.3 results for steel devices is explained. In fact, the only device that it successfully characterized is the complementary steel resonator device, therefore the detailed explanation belongs to that.

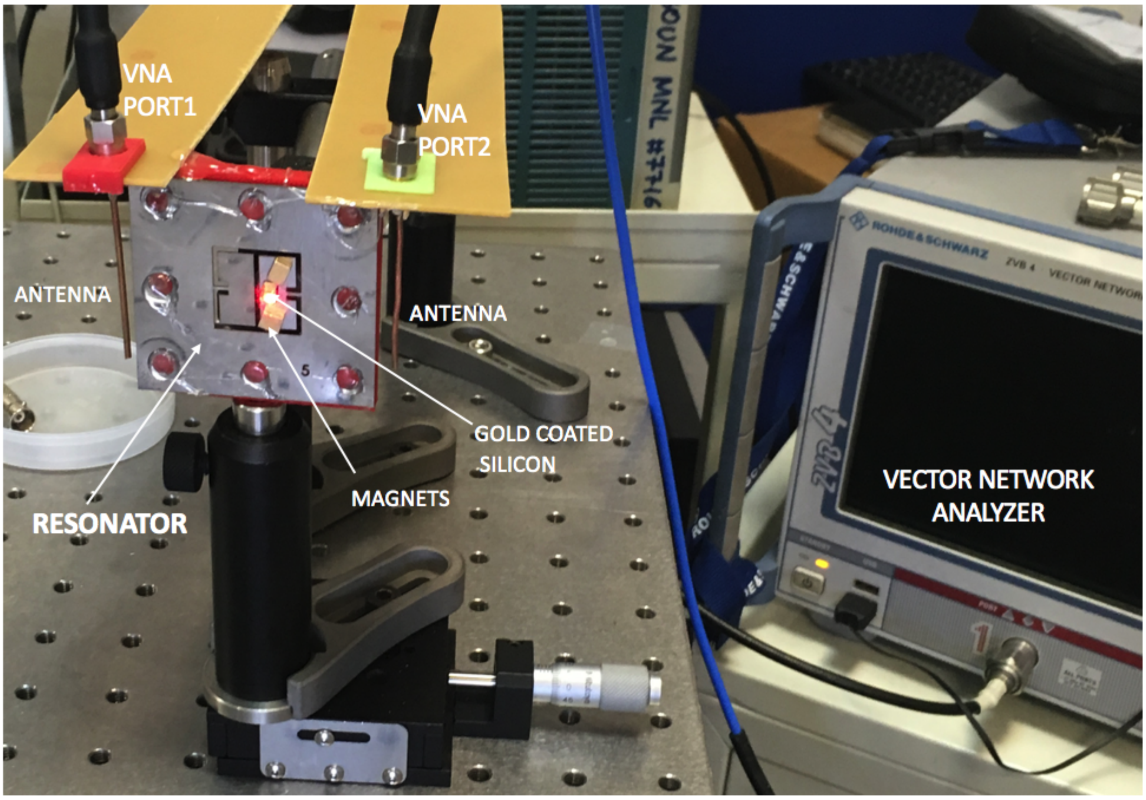

Figure 4.4. Measurement setup-2.

4.2.1. Initial Generation Resonators - Measurement

Two types of resonators are fabricated initially. Nickel layer releasing step is not successful, therefore two measurement is realized related to first bunch of resonators. Resonance frequencies of two resonator structures is measured with vector network analyzer. CST Microwave studio program is used to simulate structures. Figure 4.5 demonstrate response of measurement for copper only and nickel electroplated copper layer respectively for the single gap split ring resonator the sample design. Resonance frequency information of resonators could be taken from the S11 and S22 reflection parameters. The S21 value could not be measured.

In Figure 4.6, results for the nested gap structure is given as in the same order. In Table 4.1, summary of the simulation and measurement results is tabulated, numbers represents resonators and respective measurement layers (1) Single Gap SRR Copper

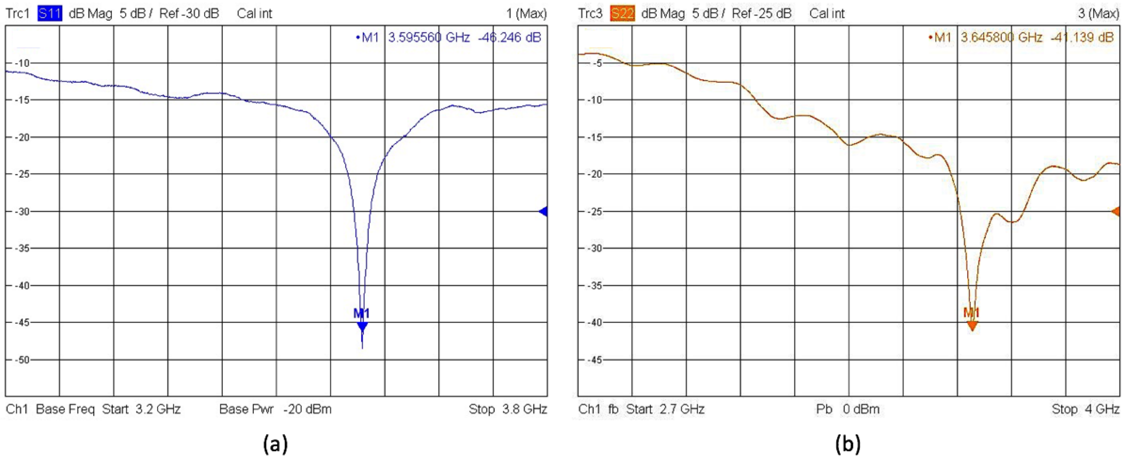

Figure 4.5. Single gap SRR S11 and S22 reflection measurement result.(a) copper only structure. (b) nickel electroplated copper structure.

Layer, (2) Single Gap SRR Nickel On Copper Layer, (3) Nested Gap SRR Copper Layer and (4) Nested Gap SRR Nickel on Copper Layer.

Table 4.1, hand calculation results for the resonance frequencies of two designs are also given. The relative errors shows the accuracy between calculation and simulation. Measurement numbers are significantly caught by the simulation and calculation for copper only structures and nickel electroplated copper structures. The error for the calculated and measured nested gap SRR case is a high value, that is 11%. There might be some additional effects on the surface charges, because of the shape of the gap is not accurate enough to be sure about electric field and surface charges.

Table 4.1. Single gap SRR measurement, calculation and simulation results.

	$f_{calculation}$	f_{sim}	f_{meas}	$Error_{calculation}$	$Error_{simulation}$
(1)	3.529	3.474	3.596	2 %	3.3 %
(2)	3.600	3.693	3.646	1.2 %	-1.2 %
(3)	3.713	3.192	3.317	-11 %	3.7 %
(4)	3.776	3.624	3.600	4.8 %	-0.6 %

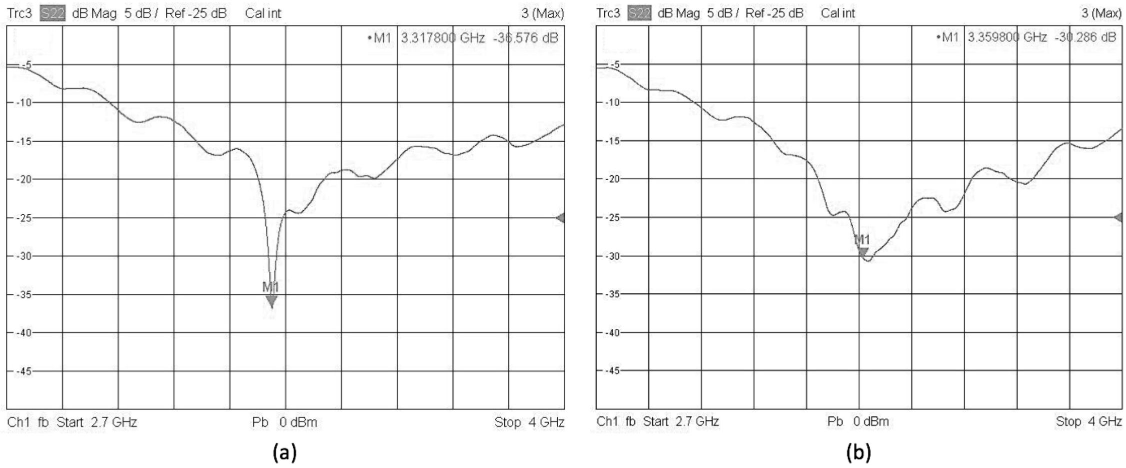

Figure 4.6. Nested gap S22 reflection measurement result.(a) copper only structure. (b) nickel electroplated copper structure.

4.2.2. Three Dimensionally Generated Resonator - Measurement

Three dimensionally fabricated resonator device has been broken during measurements. Even if the measurement could not be completed, there exists some results could be caught. Chromium, gold and nickel plated resonator's resonance frequency is measured with the setup shown in previous pictures. Shift in the resonance frequency under magnetic force is observed by bringing a magnet closer to the resonator 's cantilevers. Response of the resonator in steady state and with the magnet can be seen in Figure 4.7.

It is extracted from the measurement that for the first case the resonance frequency is 3.985 GHz, the upper frequency could not be seen however the lower frequency is about 3.84 GHz. Therefore the quality factor for the first case is calculated as 13.7. In the second case the upper frequency is close the 3.855 GHz and the lower frequency is about 3.805 GHz, so that the quality factor is calculated as 63.8 for the actuated resonator with 3.83 GHz resonance frequency.

The movement of the cantilever could not be detected clearly, there was a move in metal layer of edge parts which were not stuck to the bottom layer. Even if the

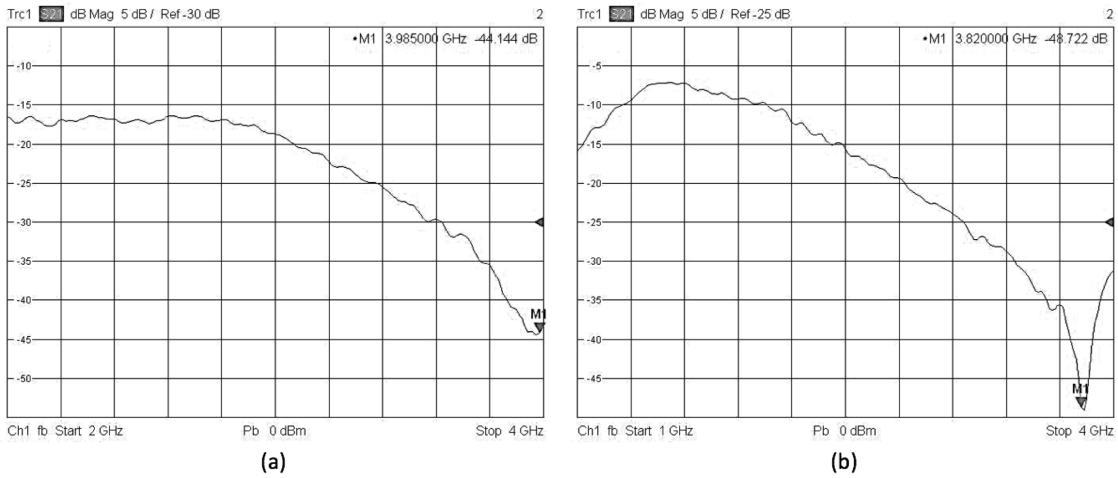

Figure 4.7. 3D generated resonator measurement. (a) in steady state (no actuation). (b) actuation with magnet.

amount of displacement could not be observed, the two picture of measurement helped to make inference about frequency shift mechanism. The relative shift of the frequency is 4.1 %.

4.2.3. Steel Resonator Measurement

In the first place, resonance frequencies are tried to be detected. The only clear response is obtained from the measurement of complementary resonator structure. Other resonators might have resonance frequencies out of the vector network analyzer measurement capability. Actually, some of the resonance frequencies are not stable at a point, they were lost for many times during study. The rest of the measurement study is about the complementary resonator structure, because of its high movement capability.

Resonance response of the resonator taken from the vector network analyzer for eight values of the excitation current applied to the electro coil are displayed in Figure 4.8.

At the time of measurement, some parameters and indicators must be carefully noted. Resonance frequency is not the only critical result for this study, it is also significant that the amount of movement of the tip of the cantilever with changing current. Movement of the cantilever is observed with the help of laser reflection setup. In each 0.1 amperes change creates nearly 5 mm shift in the reflected laser spot on the scale board.

Using this information, the angle caused from the bending is calculated using geometrical relation. From the calculated angle, displacement value of the cantilever tip is extracted. After the maximum current is achieved by the electro coil the displacement is about 15μm. Table 4.2 is prepared for complementary steel resonator measurement summary and characterization. In table, simulation for the each of the current case is given. Another critical information about the resonator is calculated frequency is 2.587 GHz, therefore the relative error for the steady state is 10.6%.

Table 4.2. Complementary steel resonator characterization.

Driving Current (A)	*Angle of Deflection (rad)*	*Cantilever Displacement (μm)*	f_{meas} *(GHz)*	f_{sim} (GHz)	*Relative error (%)*
0	-	-	2.896	3.178	- 9.7
0.300	0.285	2.24	2.884	3.002	-4.1
0.595	0.571	4.49	2.870	2.921	-1.8
0.856	0.856	6.75	2.852	2.882	-1.1
1.245	1.141	9.00	2.842	2.768	2.6
1.551	1.426	11.25	2.800	2.645	5.5
1.841	1.713	13.50	2.768	2.486	10.2
2.080	1.998	15.73	2.760	2.500	9.4

Quality factor calculated from the measurement of frequencies under changing current is displayed in Table 4.3. Quality factor of the steel resonator decreases for two of the applied currents almost in a half amount. However for the other six values, quality factor is around 90, and it does not change much. This stability shows that the resonator shows similar energy stored-energy loss behavior under tuning. The filter characteristic of the resonator also stays at same trend, so that if the resonator is used to eliminate some false signals in a circuit then it can be said that the performance of the resonator is applicable for the frequencies in the tuning range. If it is used in an oscillator circuit oscillation is also does not affected by the small change in quality factor.

Current versus frequency graph is shown in Figure 4.9. The trend in frequency against the change of electro coil current represents the overall behavior of the current controlled device. Relative amount of shift in the resonance frequency with respect to current change presents the aim of the study of making the resonator side of a current / voltage controlled oscillator circuit. Results are summarized in the Table 4.4.

Table 4.3. Quality factor for changing current values.

Current(A)	**0.0**	**0.300**	**0.595**	**0.856**	**1.245**	**1.551**	**1.841**	**2.080**
Q factor	**96.5**	**96.1**	**95.7**	**48.8**	**93.82**	**93.6**	**79.2**	**46.0**

Table 4.4. End result of steel resonator.

Current Change (A)	**Voltage Change (V)**	**Amount of Deflection (μm)**	**Frequency Change (GHz)**	**Relative Shift (%)**
2.080	**3.500**	**15.73**	**0.136**	**4.696**

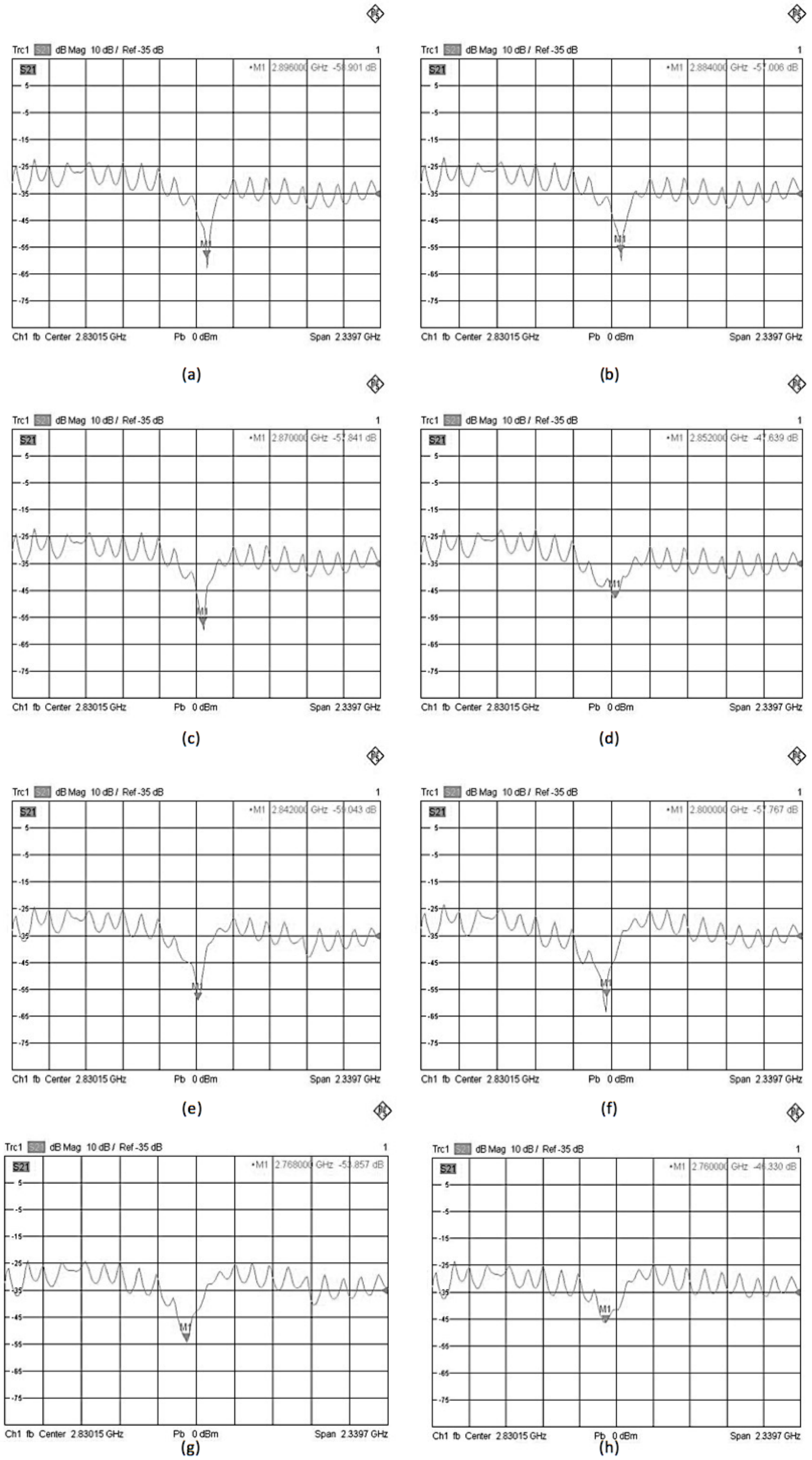

Figure 4.8. Complementary steel resonator measurement. (a) zero current (b) 0.3 A (c) 0.6 A (d) 0.9 A (e) 1.2 A (f) 1.5 A (g) 1.8 A (h) 2.1 A

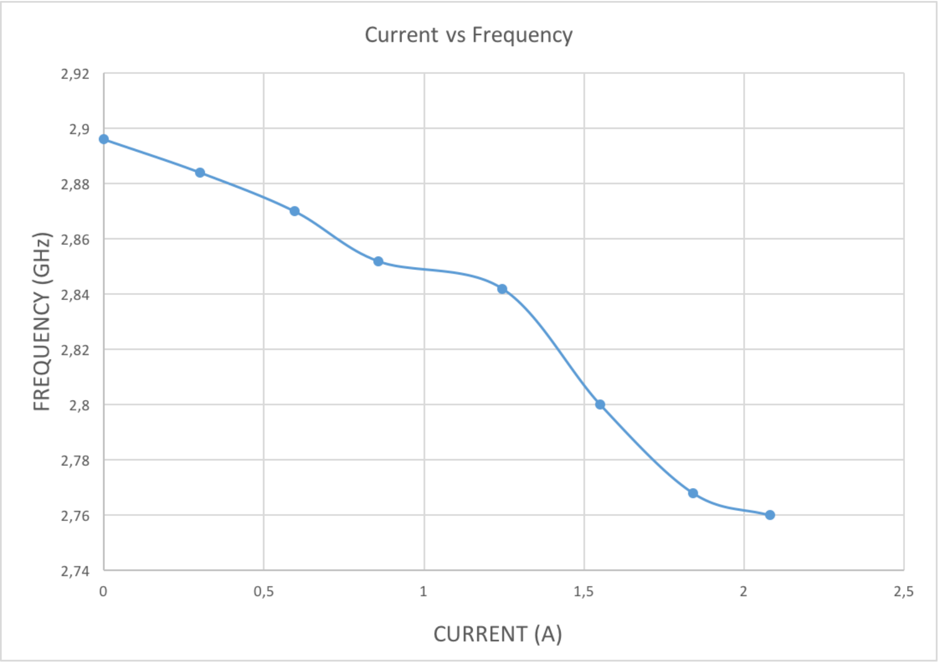

Figure 4.9. Current versus frequency.

5. CONCLUSION AND FUTURE WORK

In this study, three different designs of split ring resonators are fabricated with techniques including clean room manufacturing. Nickel layer is considered as the movable layer in the first generation resonators. Nickel electroplated structures of the first generation could not reach the final design because of the failure in the releasing step, therefore none of them represents the tunable frequency resonator. Releasing step tried to be skipped with a distinct design and fabrication method, so that three dimensionally printed resonator structure is fabricated by metal sputtering and nickel electroplating. Comparison of the measurement under constant magnetic field with steady state analysis have given hints about the effect of magnetic excitation. Steel material is chosen to eliminate all problems came across with during the experimental study. Steel resonators are designed and fabricated using laser cutter machine.

Resonance frequencies of resonators are measured, even if they are not in their final shape. To compare measurement results with CST simulation results, relative errors of the first generation resonators are lower than 16% for copper layer and nickel electroplated copper layer. Second generation resonator measurement is concluded that the shift in the resonance frequency is 4.1 % with the applied magnetic force.

Steel resonator designed as a complementary version of the ring resonator with two gaps have provided the most remarkable results among other generations. Frequency measurements are assisted by the deflection measurement setup. Resonance frequencies measured using vector network analyzer begin from 2.896 GHz and ends with 2.760 GHz. If the simulation and measurement results are compared, the relative error is found as 10.2% maximum. At that time excitation current changes from 0 A to 2.080 A. Based on these results, overall efficiency of the resonator as a part of current controlled oscillator circuit is the 4.7%. Efficiency of a convenient current controlled oscillator have to be higher than this value, however in this thesis it can be counted as good enough.

The study brought to a particular stage in this thesis can be improved by diversified approaches in summarized steps. Structural design of the resonator might be changed to a better one increasing the ability of movement of the cantilevers. Anchors can be redesigned that longer or thinner anchors provide a smaller spring constant to have noteworthy deflection. In fabrication, different materials might be selected instead of copper coated FR-4, thus problems about releasing might be handled.

Steel material has a great advantage about making structures that can be excited through magnetic field. Several thicknesses of steel plate can give the opportunity of discovering aspects of using such a material in radio frequency and microwave frequency studies. In addition to this, improved designs might be employed in biosensor applications. Measurement setup can be supported with supplementary components. A read circuit with worked data of network analyzer might create a useful voltage controlled oscillator circuit.

REFERENCES

1. Nguyen, C.-C. and R. T. Howe, "An integrated CMOS micromechanical resonator high-Q oscillator", *IEEE Journal of Solid-State Circuits*, Vol. 34, No. 4, pp. 440–455, 1999.

2. Jaakkola, A., *Piezoelectrically transduced temperature compensated silicon resonators for timing and frequency reference applications*, Ph.D. Thesis, Aalto University, 2016.

3. Wunsch, A. D., *Complex variables with applications*, Vol. 204, Addison-Wesley Reading, MA, 1983.

4. Bahl, I. J., *Lumped elements for RF and microwave circuits*, Artech house, 2003.

5. Glover, I. A., S. Pennock and P. Shepherd, *Microwave Devices, Circuits and Subsystems for Communications Engineering*, John Wiley & Sons, 2006.

6. van de Plassche, R. J., J. Huijsing and W. M. Sansen, *Analog Circuit Design: RF analog-to-digital converters; sensor and actuator interfaces; low-noise oscillators, PLLs and synthesizers*, Springer Science & Business Media, 2013.

7. Martin, T. L., *Electronic Circuits*, Prentice-Hall, 1955.

8. Gottlieb, I., *Practical oscillator handbook*, Elsevier, 1997.

9. Lee, H., J. Park and H. Lee, "Design of double negative metamaterial absorber cells using electromagnetic-field coupled resonators", *Microwave Conference Proceedings (APMC), 2011 Asia-Pacific*, pp. 1062–1065, IEEE, 2011.

10. Azad, A. K., A. J. Taylor, E. Smirnova and J. F. O'Hara, "Characterization and analysis of terahertz metamaterials based on rectangular split-ring resonators",

Applied Physics Letters, Vol. 92, No. 1, p. 011119, 2008.

11. Hajjaj, A. Z., A. Ramini, N. Alcheikh and M. I. Younis, "Electrothermally tunable arch resonator", *Journal of Microelectromechanical Systems*, Vol. 26, No. 4, pp. 837–845, 2017.

12. Vidiborskiy, A., V. Koshelets, L. Filippenko, S. Shitov and A. Ustinov, "Compacted tunable split-ring resonators", *Applied Physics Letters*, Vol. 103, No. 16, p. 162602, 2013.

13. Odyniec, M., *RF and microwave oscillator design*, Artech House, 2002.

14. Graf, R. F., *Oscillator circuits*, Elsevier, 1996.

15. Gonzalez, G., *Foundations of oscillator circuit design*, Artech house, 2007.

16. Park, S. W., *Oscillator Architectures and Enhanced Frequency Synthesizer*, Ph.D. Thesis, Texas A&M University, 2009.

17. Pozar, D. M., *Microwave Engineering*, John Wiley & Sons, 2009.

18. Razavi, B., *Fundamentals of Microelectronics*, John Wiley High Education, 2009.

19. Strauss, L., *Wave generation and shaping*, McGraw-Hill, 1960.

20. Grebennikov, A., *RF and microwave transistor oscillator design*, John Wiley & Sons, 2007.

21. Schubert Jr, T. F. and E. M. Kim, "Fundamentals of Electronics: Book 4 Oscillators and Advanced Electronics Topics", *Synthesis Lectures on Digital Circuits and Systems*, Vol. 11, No. 2, pp. 1–266, 2016.

22. Ayten, U., M. Sagbas and H. Sedef, "Electronically tunable sinusoidal oscillator circuit with current and voltage outputs", *International Journal of Electronics*,

Vol. 99, No. 8, pp. 1133–1144, 2012.

23. Gardiol, F. E., *Microstrip circuits*, LEMA-BOOK-1994-001, New York: Wiley, 1994.

24. Gautier, J.-L., *Design of microwave active devices*, John Wiley & Sons, 2014.

25. Tiebout, M., *Low power VCO design in CMOS*, Vol. 20, Springer Science & Business Media, 2006.

26. Rivera, I. F., *RF MEMS Resonators for Mass Sensing Applications*, University of South Florida, 2015.

27. Yeom, K.-W., *Microwave Circuit Design: A Practical Approach Using ADS*, Prentice Hall Press, 2015.

28. Abrams, R. L. and A. N. Chester, “Resonator theory for hollow waveguide lasers”, *Applied optics*, Vol. 13, No. 9, pp. 2117–2125, 1974.

29. Makimoto, M. and S. Yamashita, *Microwave resonators and filters for wireless communication: theory, design and application*, Vol. 4, Springer Science & Business Media, 2013.

30. Suzuki, Y., H. Shimizu, M. Takeuchi, K. Nakamura and A. Yamada, “Some studies on SAW resonators and multiple-mode filters”, *1976 Ultrasonics Symposium*, pp. 297–302, IEEE, 1976.

31. Wilson, P., *The circuit designer’s companion*, Newnes, 2017.

32. Rebeiz, G. M., *RF MEMS: theory, design, and technology*, John Wiley & Sons, 2004.

33. Bunch, J. S., A. M. Van Der Zande, S. S. Verbridge, I. W. Frank, D. M. Tanenbaum, J. M. Parpia, H. G. Craighead and P. L. McEuen, “Electromechanical resonators

from graphene sheets", *Science*, Vol. 315, No. 5811, pp. 490–493, 2007.

34. Lakin, K. M., "Thin film resonator technology", *IEEE transactions on ultrasonics, ferroelectrics, and frequency control*, Vol. 52, No. 5, pp. 707–716, 2005.

35. Mestrom, R. M., R. H. Fey and H. Nijmeijer, "Phase feedback for nonlinear MEM resonators in oscillator circuits", *IEEE/ASME Transactions on Mechatronics*, Vol. 14, No. 4, pp. 423–433, 2009.

36. Wong, T. A. and M. Palaniapan, "Micromechanical oscillator circuits: theory and analysis", *Analog Integrated Circuits and Signal Processing*, Vol. 59, No. 1, pp. 21–30, 2009.

37. Mareschal, O., S. Loiseau, A. Fougerat, L. Valbin, G. Lissorgues, S. Saez, C. Dolabdjian, R. Bouregba and G. Poullain, "Piezoelectric aluminum nitride resonator for oscillator", *IEEE transactions on ultrasonics, ferroelectrics, and frequency control*, Vol. 57, No. 3, pp. 513–517, 2010.

38. Sydoruk, O., E. Tatartschuk, E. Shamonina and L. Solymar, "Analytical formulation for the resonant frequency of split rings", *Journal of applied physics*, Vol. 105, No. 1, p. 014903, 2009.

39. Walls, F. L. and J. R. Vig, "Fundamental limits on the frequency stabilities of crystal oscillators", *IEEE transactions on ultrasonics, ferroelectrics, and frequency control*, Vol. 42, No. 4, pp. 576–589, 1995.

40. Zhu, W., H. Cai, T. Mei, T. Bourouina, J. Tao, G. Lo, D. Kwong and A. Liu, "A MEMS tunable metamaterial filter", *Micro Electro Mechanical Systems (MEMS), 2010 IEEE 23rd International Conference on*, pp. 196–199, IEEE, 2010.

41. Ozbey, B. and O. Aktas, "Continuously tunable terahertz metamaterial employing magnetically actuated cantilevers", *Optics express*, Vol. 19, No. 7, pp. 5741–5752, 2011.

42. Withayachumnankul, W., C. Fumeaux and D. Abbott, “Compact electric-LC resonators for metamaterials”, *Optics express*, Vol. 18, No. 25, pp. 25912–25921, 2010.

43. Munina, I., V. Turgaliev and I. Vendik, “Tunable terahertz metamaterials based on electrically controlled piezoelectric actuators”, *Technical Physics Letters*, Vol. 38, No. 6, pp. 579–582, 2012.

44. Dhouibi, A., S. N. Burokur, A. de Lustrac and A. Priou, “Comparison of compact electric-LC resonators for negative permittivity metamaterials”, *Microwave and Optical Technology Letters*, Vol. 54, No. 10, pp. 2287–2295, 2012.

45. Cai, W., U. K. Chettiar, A. V. Kildishev and V. M. Shalaev, “Optical cloaking with metamaterials”, *Nature photonics*, Vol. 1, No. 4, pp. 224–227, 2007.

46. Landy, N. I., S. Sajuyigbe, J. Mock, D. Smith and W. Padilla, “Perfect metamaterial absorber”, *Physical review letters*, Vol. 100, No. 20, p. 207402, 2008.

47. Arritt, B., B. Adomanis, T. Khraishi and D. Smith, “Parametric analysis of the strain-dependent behavior of a metamaterial electric resonator”, *Applied Physics Letters*, Vol. 97, No. 19, p. 191907, 2010.

48. Li, X. M., J. Yu, P. Li, J. J. Yang and M. Huang, “Metamaterial-inspired sensor based on a complementary asymmetric double-split resonator”, *Electronic Information and Communication Technology (ICEICT), IEEE International Conference on*, pp. 424–427, IEEE, 2016.

49. Odabasi, H. and F. Teixeira, “Electric-field-coupled resonators as metamaterial loadings for waveguide miniaturization”, *Journal of Applied Physics*, Vol. 114, No. 21, p. 214901, 2013.

50. Saha, C. and J. Siddiqui, “Estimation of the resonance frequency of conventional and rotational circular split ring resonators”, *Applied Electromagnetics Conference (AEMC), 2009*, pp. 1–3, IEEE, 2009.

51. Bilotti, F., A. Toscano, L. Vegni, K. Aydin, K. B. Alici and E. Ozbay, "Equivalent-circuit models for the design of metamaterials based on artificial magnetic inclusions", *IEEE Transactions on Microwave Theory and Techniques*, Vol. 55, No. 12, pp. 2865–2873, 2007.

52. Young, W. C. and R. G. Budynas, *Roark's formulas for stress and strain*, Vol. 7, McGraw-Hill New York, 2002.

53. Spasos, M. and R. Nilavalan, "Ohmic RF-MEMS Control", *Materials and Failures in MEMS and NEMS*, pp. 239–262, John Wiley & Sons, Inc., 2015.

54. Zhang, X. and Y. Wu, "Effective medium theory for anisotropic metamaterials", *Scientific reports*, Vol. 5, 2015.

55. Héctor, J., *RF MEMS circuit design for wireless communications*, Artech House, 2002.

56. Fedder, G. K., C. Hierold, J. G. Korvink and O. Tabata, *Resonant mems: Fundamentals, implementation, and application*, John Wiley & Sons, 2015.

57. Carlsson, E. and S. Gevorgian, "Conformal mapping of the field and charge distributions in multilayered substrate CPWs", *IEEE Transactions on Microwave Theory and Techniques*, Vol. 47, No. 8, pp. 1544–1552, 1999.

58. Jiang, Y., G. Li, Z. Liang and F. Guo, "Calculation of Power Frequency Electric Field under Overhead Lines with Sloping Ground by Conformal Mapping", *Information Science and Control Engineering (ICISCE), 2015 2nd International Conference on*, pp. 645–648, IEEE, 2015.

59. Olver, P. J., "Complex analysis and conformal mapping", *University of Minnesota*, 2015.

60. Delgado, V., O. Sydoruk, E. Tatartschuk, R. Marqués, M. Freire and L. Jelinek,

"Analytical circuit model for split ring resonators in the far infrared and optical frequency range", *Metamaterials*, Vol. 3, No. 2, pp. 57–62, 2009.

61. Brown, J. W. and V. R. Churchill, *Complex variables and applications*, Boston: McGraw-Hill Higher Education, 2009.

62. Serway, R. A. and J. W. Jewett, *Physics for scientists and engineers with modern physics*, Cengage learning, 2018.

63. Studio, M., "CST-Computer Simulation Technology", *Bad Nuheimer Str*, Vol. 19, p. 64289, 2008.

64. Lee, H., "Absorption Bandwidth-Enhanced Metamaterial Absorber Using Inplaned ELC Resonator and Cut-Wire", *Electrical and Electronic Engineering*, Vol. 4, No. 4, pp. 73–79, 2014.

65. Schwartz, M., "Deposition from aqueous solutions: an overview", *Handbook of Deposition Technologies for Films and Coatings Science, Technology and Applications*, p. 506, 1994.

66. Di Bari, G. A., "Electrodeposition of nickel", *Modern electroplating*, Vol. 5, pp. 79–114, 2000.

67. Kanani, N., *Electroplating: basic principles, processes and practice*, Elsevier, 2004.

68. Baudrand, D., "EL Nickel Plating", *ASM Handbook, Surface Engineering*, Vol. 5, p. 290, 1994.

69. Luo, J., M. Pritschow, A. Flewitt, S. Spearing, N. Fleck and W. Milne, "Effects of process conditions on properties of electroplated Ni thin films for microsystem applications", *Journal of the Electrochemical Society*, Vol. 153, No. 10, pp. D155–D161, 2006.

70. Castañer, L., *Understanding MEMS: Principles and Applications*, John Wiley &

Sons, 2015.

71. Mack, C., *Fundamental principles of optical lithography: the science of microfabrication*, John Wiley & Sons, 2008.

72. Le Tiec, Y., *Chemistry in Microelectronics*, John Wiley & Sons, 2013.

73. Zhao, Z., J. Gallman and R. White, "Micromachined Nickel Floating Element Shear Stress Sensor Array", *ECS Transactions*, Vol. 41, No. 20, pp. 19–25, 2012.

74. Zeltmann, S. E., N. Gupta, N. G. Tsoutsos, M. Maniatakos, J. Rajendran and R. Karri, "Manufacturing and security challenges in 3D printing", *The Journal of The Minerals*, Vol. 68, No. 7, pp. 1872–1881, 2016.

75. Alfonso, E., J. Olaya and G. Cubillos, "Thin film growth through sputtering technique and its applications", *Crystallization-Science and Technology*, InTech, 2012.

76. Depla, D., S. Mahieu and J. Greene, "Sputter deposition processes", *Handbook of Deposition Technologies for Films and Coatings (Third Edition)*, pp. 253–296, Elsevier, 2010.

77. Cheng, D. K., *Fundamentals of engineering electromagnetics*, Pearson Education, 1993.